ISSN 0255-7193

CLAY RESEARCH

Vol. 36, No. 1

June, 2017

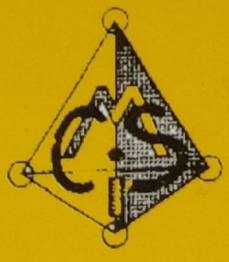

IOS Press

Overseas distribution
IOS Press, The Netherlands

THE CLAY MINERALS SOCIETY OF INDIA
Division of Soil Science and
Agricultural Chemistry
Indian Agricultural Research Institute
New Delhi-110 012, India

Overseas subscribers may send
their queries to IOS Press, Nieuwe
Hemweg 6B, 1013 BG Amsterdam,
The Netherlands, orders@iospress.in:
URL: http://www.iospress.nl

THE CLAY MINERALS SOCIETY OF INDIA

(Registered under Act XXI of 1860)
Registration No. S/13028 of 1982

COUNCIL FOR 2016

President	:	Dr. S.K. Singh
Vice Presidents	:	Dr. D.C. Nayak
		Dr. Nayan Ahmed
Secretary	:	Dr. S.K. Mahapatra
Joint Secretaries	:	Dr. Gautam Goswami
		Dr. Sudarshan Dutta
Treasurer	:	Dr. Jaya N. Surya
Chief Editor	:	Dr. S.C. Datta
Editors	:	Dr. K. M. Manjaih
		Dr. S.K. Roy
		Dr. P. Chandran
Councilor	:	East zone : Dr. A.K. Sahoo, Dr. Siladitya Bandopadhyay
Councilor	:	West zone : Dr. A.L. Pharande, Dr. Vilas kharche
Councilor	:	North zone : Dr. U.K Maurya, Dr. B.N. Ghosh
Councilor	:	South zone : Dr. K.S. Anil Kumar, Dr. Chandrakala M.
Councilor	:	Central zone : Dr. P. Chandran, Dr. Tapan Adhikari
Past Presidents	:	Dr S.K. Mukherjee, Dr K.V. Raman, Dr S.K. Ghosh, Dr. D.K. Pal, Dr. Dipak Sarkar

EDITORIAL BOARD

International Consulting Editor	:	Dr. S.R. Krishnamurti Gummuluru Adjunct Associate Professor, CERAR, University of South Australia, Canada Dr. Sridhar Komarneni Adjunct Professor of Civil and Environmental Engineering & Editor-in-Chief, J. Porous Materials, USA

Annual Institutional Subscription Rates Inclusive of Air Mail and Handling Charges :

Subscription Rates (Year 2011)	Indian (INR)	Overseas (USD)
Print + online access	Rs. 1,800.00	$ 350.00
Online access	Rs. 600.00	$ 150.00
Print	Rs. 1,200.00	$ 200.00

All payments should be sent to **"The Clay Minerals Society of India"** Division of Soil Science and Agricultural Chemistry, I.A.R.I., New Delhi-110 012

Clay Research, Vol. 36, No. 1, pp. 1-16 (2017)

Fourth Professor SK Mukherjee –
The Clay Minerals Society of India Foundation Lecture

Clay Mineral Equilibria : Fuzzy Phase Diagrams

CHANDRIKA VARADACHARI

Raman Centre for Applied and Interdisciplinary Sciences, 16A Jheel Road, Kolkata 700 075

It is indeed an honour to present the Fourth CMSI Foundation Lecture in memory of Professor Sushil Kumar Mukherjee, Founder President of the society. Professor Mukherjee was one of the founding fathers of clay physical chemistry in India, initiated by his teacher Professor J.N. Mukherjee, with monumental contributions in the field of clay membranes, clay acidity and Donnan equilibria. As a token of my deep respect and gratitude, I dedicate this new area of research in clay thermodynamics, to Professor S.K. Mukherjee.

Introduction

Clay minerals are the most abundant inorganic materials on the surface of the Earth. They form the outer layer or skin of the Earth and are also found in extraterrestrial bodies like meteorites, asteroids and interplanetary dust particles. Since clay minerals constitute the bulk of most soils, they function as the nutrient store for plants, trapping and releasing nutrients, storing water, providing a support for roots and habitat for countless soil flora and fauna. Apart from agriculture, the importance of clay minerals extends across various industries including chemical, petrochemical, pharmaceutical, mining, etc.; additionally clay minerals may be considered the womb of life, since life originated from the support and catalytic base provided by clays.

Clay minerals are macromolecular structures formed by the combination of silica tetrahedra and aluminium octahedra, with numerous substitutions in both. Substitutions of silicon and aluminium form the basis of charge in the mineral, which is a combination of the tetrahedral and octahedral charges. Substitutions also result in different types of clay minerals that have widely different physico-chemical properties and extremely complex compositions. Compositional diffuseness together with variation in structural charges, create a major hurdle in the study of clay mineral thermodynamics at every stage of study.

Challenges in theoretical phase diagrams and thermodynamics

Phase diagrams provide a graphical representation of the environmental conditions under which (i) clay minerals would be neoformed in soils and aquatic systems, (ii) they would be stable or unstable and (iii) the transformation routes and end products of weathering as influenced by the environment. Therefore, theoretical phase diagrams provide the geochemical history of clay minerals and are immensely supportive tools in mineralogy, pedology and geochemistry. Challenges in theoretical modeling of clay mineral phase diagrams are present at three levels.

(a) Compositional complexity and classification

Classification of the clay minerals at the

***Corresponding Author Email :** cv@rcais.res.in

highest level, into the 1:1, 2:1 and 2:2 clays depending on the ratio of silica tetrahedral sheet to alumina/magnesia octahedral sheet, is quite easily done based on their crystallographic properties (Fig. 1). Similarly, group level classification can also be done based on crystallographic and physico-chemical properties. Thus, the 2:1 minerals are classified into clay micas, smectites and vermiculites (Newman, 1987). Classification at the subgroup level presents a formidable problem. This is particularly because a conjunction of numerous tools must be used and compositional data alone are of little use in classification. To add to the difficulty, there is no consensus on whether clay minerals are compositionally distinct entities or are simply solid solutions forming a series from one compositional extreme to another. With hundreds of compositions for each type of clay mineral and no representative composition defining each type of mineral, thermodynamic modeling becomes very subjective.

(b) Standard free energy of formation

Experimental methods for evaluating standard free energy of formation (ΔG°_f) of clay minerals are extremely time consuming and, therefore, this has restricted the availability of ΔG°_f data to just a few minerals. It is actually impossible to obtain experimental values of ΔG°_f for the innumerable compositions that exist in nature.

To overcome this problem, theoretical methods have been developed (Chen, 1975; Nriagu, 1975; Slaughter 1966; Sposito, 1986; Tardy and Garrels, 1974, 1977). These methods were limited in their applicability to different clay mineral compositions or did not provide sufficiently accurate results. A reliable theoretical method is a prerequisite to any thermodynamic

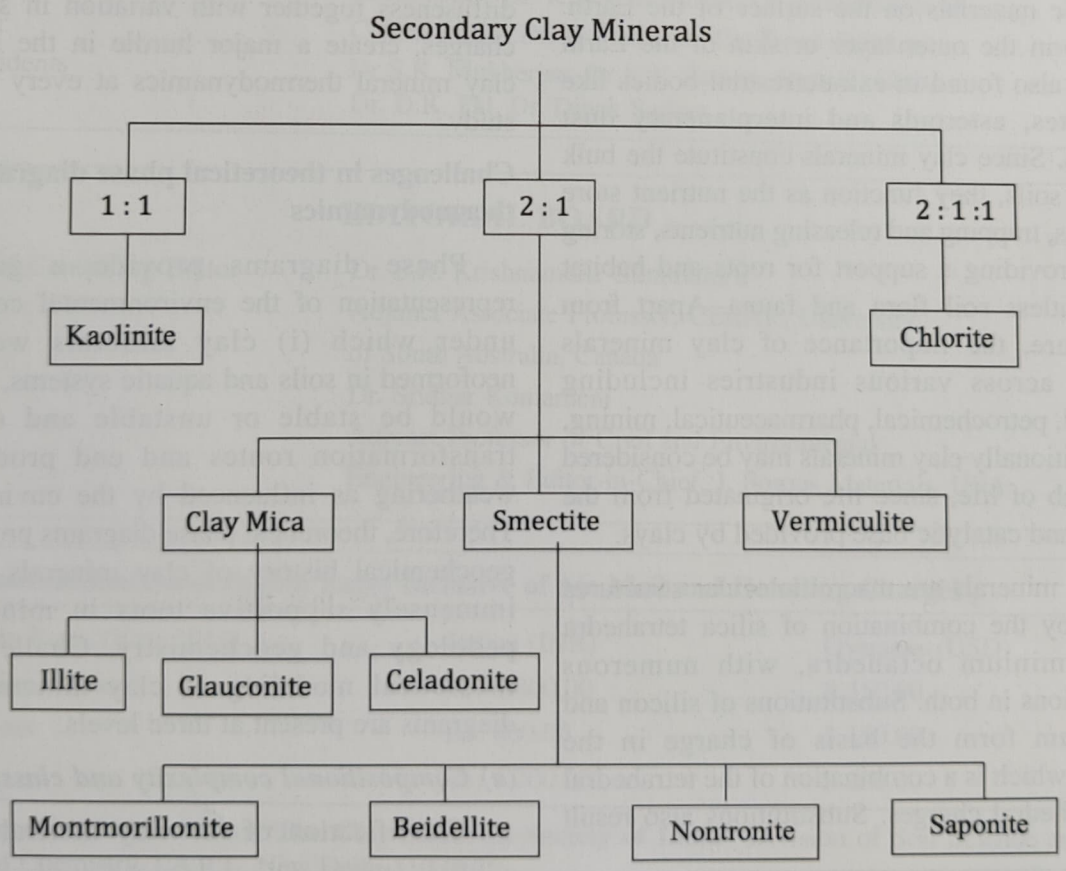

Fig. 1. *Broad group and subgroup of clay minerals*

calculations of mineral equilibria.

(c) Phase diagrams

The primary drawback in derivation of clay mineral phase diagrams was that the popular method as developed by Garrels and Christ (1965) was fundamentally flawed. It violated some of the fundamental principles of the Phase Rule. These limitations of this method have been discussed in detail by Varadachari and Ghosh (2003) and are discussed here briefly.

The Phase Rule states that for any system in equilibrium, F=C-P+2, where F is the degree of freedom, C is the components and P is the phases in equilibrium. In oxidising environments, the following major components contribute to the equilibrium, viz., $Si(OH)_4$, $Al(OH)_3$, FeO(OH), Ca^{2+}, Mg^{2+}, K^+, H^+, H_2O and the clay mineral itself (C = 9). The phases, P, in such a system is 4, i.e., $Al(OH)_3$, FeO(OH), clay mineral and the aqueous phase. Therefore, the degrees of freedom in this system F = 7. If pressure and temperature (P-T) are fixed at ambient, then Phase Rule requires that the system has 5 degrees of freedom. Therefore according to the Phase Rule, the equilibrium in such a system containing a clay mineral (at constant P, T) has to be defined by at least 5 parameters which are the major ionic constituents of soil solutions, viz., $Si(OH)_4$, Ca^{2+}, Mg^{2+}, K^+ and H^+. It follows that in a $\log[Si(OH)_4 - \log(K^+/H^+)]$ representation (commonly used by Garrels and Christ, 1965), the parameters $\log[Mg^{2+}/(H^+)^2]$ and $\log[Ca^{2+}/(H^+)^2]$, must have defined values. Previous workers who have derived mineral equilibrium diagrams (Aagard and Helgeson, 1983; Garrels and Christ, 1965; Helgeson *et al.,* 1969) defined the systems by only two parameters such as, $\log[Si(OH)_4]$-$\log[K^+/H^+]$ or $\log[Si(OH)_4]$- $\log[Mg^{2+}/(H^+)^2]$, etc. Equilibrium diagrams constructed this way do not comply with the Phase Rule. Secondly, the theoretical derivation of phase diagrams requires that for 'n' minerals, ${}^nC_2$ + n equilibrium lines have to be evaluated (all possible mineral pairs + mineral-solution equilibria). This process has not been followed by previous workers (Garrels and Christ, 1965).

Hence, the diagrams derived by them are not phase diagrams but are only representation of equilibrium lines for selected pairs of mineral equilibria. Only when all possible equilibria are considered, the actual free energy minimum can be derived. In such a free energy minimum state, one or more minerals may not be represented in phase diagrams because they are thermodynamically less stable phases. However, in equilibrium diagrams described by earlier workers (Garrels and Christ, 1965; Helgeson *et al.,* 1969), no mineral is excluded because their process does not derive the minimum free energy state of the system. Therefore, the Garrels and Christ (1965) method only defines equilibrium boundaries between arbitrary pairs of minerals and does not derive the system with lowest free energy state. For the same reason, the earlier methodology could not derive metastable and unstable mineral phases.

The method continued to be used for several decades by numerous workers (Helgeson *et al.*, 1969; Tardy and Duplay, 1994). To find a solution to the limitations of the earlier methodology, a new concept is required for phase diagram derivation. This new method ought to be theoretically correct and confirm to all aspects of the Phase Rule and should also derive metastable phases. Such a method was developed by Varadachari (1992).

The second drawback of the traditional methods was that they could not accommodate compositional variability of clay minerals. Thus in the derivations, an illite would have to be defined by a mineral of one defined composition and illites of other compositions could not be included. The third drawback of the traditional method was that they only showed pure (single) mineral phases with sharp transitions (Garrels and Christ, 1965; Helgeson *et al.*, 1969; Tardy

and Duplay, 1994). This is not representative of soil and aqueous environments where mixed mineral assemblages are common and mineral transitions are gradual.

In order to further overcome these limitations, the basic mathematical treatment required to be changed. Traditional mathematical methods that assume crisp and precise situations would have to be replaced with fuzzy mathematics that can handle the vagueness in clay mineral compositions and diffuseness of mineral occurrences. Such a method was developed by Varadachari (2006) and is briefly described in later sections.

Overcoming the challenges

The solution to problems in deriving phase diagrams of clay minerals had to be done at three levels. The first level was to enable statistical and mathematical treatment of clay mineral compositions in preparation for fuzzy mathematical treatment. At this level, we had to study compositional variations to enable clay mineral classifications and groupings and to derive ideal, representative formulae for each type of mineral. The second level was to theoretically derive standard free energy of formation values (ΔG°_f). The theoretical method would have to be applicable to all types of clay minerals and provide accurate results. These two levels provided the basic groundwork for ultimately deriving a fuzzy phase diagram.

(a) Clay mineral classification and grading

(i) Are groups and subgroups compositionally discrete and distinguishable?

It is crucial to understand if clay mineral compositions form a continuous series from one end member to another or form discrete compositional clusters. We used a statistical pattern recognition tool, discriminant analysis, to analyse the compositions of 464 clay minerals (Varadachari and Mukherjee, 2004). This statistical technique (i) allowed us to select the chemical parameters that distinguish groups and subgroups of clay minerals, (ii) showed that each group and subgroup form compositional clusters and are not a continuous series of solid solutions, (iii) led to the development of a statistical model of a representative composition for each mineral and (iv) derived a simple equation for group and subgroup classification of any clay mineral from its composition data alone.

Discriminant analysis showed that just two parameters, viz., total layer charge (TLC) and K content can distinguish three groups of 2:1 minerals, viz., smectite, clay mica and vermiculite (Table 1). For further subgroup level differentiation, only four parameters are required (Table 2), viz., tetrahedral charge (TC), octahedral charge (OC), tetrahedral Al (^{IV}Al) and octahedral Mg (^{VI}Mg). Derivation shows that at the subgroup level, there are only three clay micas (illite, glauconite and celadonite) and four smectites (montmorillonite, beidellite, nontronite and saponite). The accuracy of predicted classifications was 85-95% compared to experimental values. Squared Mahalanobis distances between the mineral compositions were highly significant (0.0001%). Thus, discriminant analysis proved that clay minerals have chemically distinct compositional clusters with clear distinguishable features that separate each type (Varadachari and Mukherjee, 2004).

(ii) Can they be classified by compositions alone?

A simple computational procedure was developed to derive the group and subgroup level classification of a clay mineral based only on its composition data (Varadachari and Mukherjee, 2004). The formula for deriving broad group classification based on these two parameters is shown in Table 1 and the formulae for deriving subgroup level classifications are shown in Table 2. The step-by-step process is described in Mukherjee *et al.* (2006a). It consists in deriving the "classification scores" of a mineral in various

groups. The mineral is classified into that group in which it has the highest score. For example, a mineral was found to have a classification score of 5.03 in clay mica group, 2.02 in smectite group and -10.59 in vermiculite group; therefore, it is a clay mica (the mineral used in the example was in fact an illite). Similarly, the same mineral had classification scores of 43.49 in illite subgroup, 40.00 in glauconite subgroup and 33.36 in celadonite subgroup; therefore, it belongs to the illite subgroup (Mukherjee *et al.*, 2006a).

(iii) Can we have a representative formula for each subgroup of clay mineral?

Discriminant analysis also helped to derive the representative or "centric" formulae for each clay type (Table 3; Varadachari and Ghosh, 2009). Thus, the centric composition of montmorillonite is $K_{0.178}Na_{0.112}Ca_{0.0745}(Si_{3.823}Al_{0.177})\ Al_{1.453}Fe^{III}_{0.245}Mg_{0.322}O_{10}(OH)_2$, that for illite is $K_{0.63}Na_{0.0624}(Si_{3.447}Al_{0.553})\ Al_{1.685}\ Fe^{III}_{0.1142}\ Fe^{II}_{0.0247}\ Mg_{0.2068}O_{10}(OH)_2$ and for beidellite the formula is $K_{0.1328}Na_{0.0632}\ Ca_{0.1184}\ (Si_{3.625}Al_{0.375})Al_{1.86}\ Fe^{III}_{0.054}\ Fe^{II}_{0.0061}Mg_{0.094}O_{10}(OH)_2$.

(iv) Can we grade clay minerals compositions?

We have thus far derived methodologies for classifying minerals into groups and subgroups (such as clay mica and illite) using formulae

Table 1. *Broad group level classification*

Broad group of 2:1 Minerals	Parameters required for classification	Formula for deriving classification score
Clay Mica	x =total layer charge (TLC)	$P_{CM} = -14.1*x + 15.3*y - 10.8$
Smectite	y = potassium (K)	$P_S = -21.8*x - 11.1*y - 5.07$
Vermiculite	both from half cell formula	$P_V = -45.7*x - 35.6*y - 19.3$

Table 2. *Subgroup level classification*

Subgroup of 2:1 Minerals	Parameters required for classification	Formula for deriving classification score
Illite		$S_i = 39.3*q + 46.5*r - 37.2*s - 34.3*t - 49.2$
Glauconite	q = octahedral Al (^{VI}Al)	$S_g = 30.2*q + 48.4*r - 37.6*s - 34.3*t - 39.3$
Celadonite	r= octahedral Mg (^{VI}Mg)	$S_c = 28.3*q + 56.3*r - 38.1*s - 29.7*t - 42.7$
Montmorillonite	s= octahedral charge (OC)	$S_m = 31.8*q + 11.8*r - 21.2*s - 12.8*t$
Nontronite	t= tetrahedral charge (TC)	$S_n = 12.8*q + 6.98*r - 16.8*s - 20.4*t$
Beidelite		$S_b = 45.1*q + 11.4*r - 19.7*s - 10.0*t$
Saponite		$S_s = 21.4*q + 58.3*r - 6.2*s - 19.1*t$

Table 3. *Centric formulae of 10 different sub-groups*

Clay subgroup (Group)	Centric formula
Illite (Clay mica)	$K_{0.63}Na_{0.0624}(Si_{3.447}Al_{0.553})Al_{1.685}Fe^{III}_{0.1142}Fe^{II}_{0.0247}Mg_{0.2068}O_{10}(OH)_2$
Glauconite (Clay mica)	$K_{0.748}Na_{0.05}Ca_{0.03}\ (Si_{3.65}Al_{0.35})Al_{0.502}FeIII_{0.95}Fe^{II}_{0.148}Mg_{0.42}O_{10}(OH)_2$
Celadonite (Clay mica)	$K_{0.701}Na_{0.0755}Ca_{0.052}(Si_{3.867}Al_{0.133})Al_{0.179}FeIII_{1.0105}Fe^{II}_{0.196}Mg_{0.646}O_{10}(OH)_2$
Montmorillonite (Smectite)	$K_{0.178}Na_{0.112}Ca_{0.0745}(Si_{3.823}Al_{0.177})Al_{1.453}Fe^{III}_{0.245}Mg_{0.322}O_{10}(OH)_2$
Beidellite (Smectite)	$K_{0.1328}Na_{0.0632}Ca_{0.1184}(Si_{3.625}Al_{0.375})Al_{1.86}Fe^{III}_{0.054}FeII_{0.0061}Mg_{0.094}O_{10}(OH)_2$
Nontronite (Smectite)	$K_{0.105}Na_{0.107}Ca_{0.125}(Si_{3.592}Al_{0.408})Al_{0.052}Fe^{III}_{1.75}Mg_{0.27}O_{10}(OH)_2$
Saponite (Smectite)	$K_{0.017}Na_{0.027}Ca_{0.1895}(Si_{3.518}Al_{0.482})Al_{0.047}Fe^{III}_{0.083}Fe^{II}_{0.1105}Mg_{2.724}O_{10}(OH)_2$
Vermiculite (Vermiculite)	$Mg_{0.373}(Si_{2.81}Al_{1.19})Al_{0.086}Fe^{III}_{0.408}Mg_{2.481}O_{10}(OH)_2$
Chlorite (Chlorite)	$K_{0.01}Ca_{0.001}Mg_{0.005}(Si_{2.929}Al_{1.071})Al_{1.143}Fe^{III}_{0.244}Fe^{II}_{1.324}Mg_{3.12}O_{10}(OH)_8$

based on discriminant analysis. However, even at the subgroup level itself, minerals can show great variations in compositions. Hence, there is a need to be able to quantify the compositional differences between minerals of the same type and evaluating how "good" is a sample (or how representative of its type). This measurement is possible by assigning grades or "belongingness" to a group, derived using fuzzy mathematics (Mukherjee *et al.*, 2006b; Varadachari and Ghosh, 2009; Varadachari *et al.*, 2003). These grades are measured in a scale of 0 to 1 with 1 being the highest grade as for the typical or representative composition. For example, a good quality illite could have a high grade of 0.9 "illiteness" whereas a poor quality illite could have an illiteness of 0.3. Grading helps to select minerals which belong to that group or subgroup and are not outliers. Thus, only representative minerals can be selected for mathematical derivation of phase diagrams.

Another advantage with grading minerals is that it allows an evaluation of resemblance or likeness between minerals. Thus, it is derived that centric or representative beidellite has an "illiteness" of 0.36 (Table 4; Mukherjee *et al.*, 2006b). Amongst the three subgroups of clay mica, the "micaness" of celadonite is the highest (it is closest to the typical features of clay mica group). The overlap or resemblance of a typical illite to a typical montmorillonite is 0.27 (Table 4). Similarly, saponite has a "vermiculiteness" of 0.29.

Clay mineral grading thereby introduces a third level of clay mineral classification by distinguishing minerals of the same type. This was earlier not possible. This tool also allows an understanding of the extent of transformation of one mineral to another. Fuzzy membership grades for selected clay minerals are shown in Table 5a.

The detailed, step-wise procedure for deriving grades of clay minerals is described in Mukherjee *et al.* (2006b). The fundamental mathematics and statistical process for deriving the formulae is available in Varadachari *et al.* (2003). Thus, it became possible to describe the clay minerals mathematically and, as a result, paved the way to make them amenable to mathematical treatments.

(b) Standard free energy of formation

Computational methods for derivation of standard free energy of formation (ΔG°_f) are mostly based on combining ΔG°_f values of the component oxides followed by computations based on introduction of error terms, electronegativity parameters, etc. (Nriagu, 1975; Tardy and Garrels, 1977).

More promising methods were developed by

Table 4. *Grades of belongingness of the centric compositions of each clay mineral subgroup*

Minerals	Grades of belongingness	
	Group	Subgroup
Illite	Micaness = 0.76;	Illiteness = 1.00; Montmorilloniteness = 0.27; Beidelliteness = 0.14
Glauconite	Micaness = 0.86 ;	Glauconiteness = 1.00 ; Nontroniteness = 0.19
Celadonite	Micaness = 0.89 ;	Celadoniteness = 1.00
Montmorillonite	Smectiteness = 0.91;	Montmorilloniteness = 1.00 ; Illiteness = 0.13; Beidelliteness = 0.3
Beidellite	Smectiteness = 0.96;	Beidelliteness = 1.00 ; Illiteness = 0.36
Nontronite	Smectiteness = 0.96;	Nontroniteness = 1.00 ; Glauconiteness = 0.17
Saponite	Smectiteness = 0.86;	Saponiteness = 1.00 ; Vermiculiteness = 0.29
Vermiculite	Vermiculiteness = 1.00;	Vermiculiteness = 1.00; Saponiteness = 0.00

Karpov and Kashik (1968) and Chen (1975) based on a regression equation for deriving ΔG°_f values from the sums of the ΔG°_f of components. In the first step, the mineral is represented as a combination of various oxides and silicates from which the minerals are assumed to be formed. For each combination, the sum of ΔG°_f of the components (i.e. $\Sigma\Delta G^\circ_f$) is computed. The $\Sigma\Delta G^\circ_f$ values are arranged in descending order and each value is assigned a rank x. In the original process, the value of rank x was chosen arbitrarily. Varadachari *et al.* (1994) used a tree-diagram approach to compute possible combinations of assignment of x values.

The equation $\Sigma\Delta G^\circ_f = ae^{bx} + c$ is then solved where 'a' and 'b' are constants to be determined by regression analysis and 'c' gives the value of ΔG°_f for the mineral (Varadachari *et al.,* 1994).

Subsequently, curvilinear regression curve fitting was done to obtain the combination of x values that produced the best fit and the value of ΔG°_f was obtained from that equation. An iterative least square fit procedure was used with some initial estimates of *a, b* and *c* and estimation of the error $\Sigma\varepsilon^2$; iteration was continued till the solution converged (Kudrat *et al.,* 1999; Varadachari *et al.,* 1994). A computer program (Kudrat *et al.,* 1999) was developed for derivation of ΔG°_f of clay minerals. This program can be downloaded from https://www.iamg.org/index.php/publisher/articleview/frmArticleID/112 and is available for UNIX systems (C language) as well as for X-Windows systems. Computed values showed excellent fit in minerals whose experimental values are available. Thus, derived values of ΔG°_f of kaolinite and muscovite are -905.121 and -1337.991 kcal/mole for which experimental values are -905.614 and - 1336.301 kcal/mole respectively (Kudrat *et al.,* 1999). Later Kudrat *et al.* (2000) used this methodology to derive the ΔG°_f of a large number of non-stoichiometric clays belonging to the illite, smectite, vermiculite and chlorite groups. Values of ΔG°_f for few such clay minerals are shown in Table 5a. They also studied the correlations of ΔG°_f values with compositional parameters. The ΔG°_f of illites correlated strongly with octahedral Al (Al^{VI}), becoming more negative with increasing Al^{VI} and less negative with increasing Fe^{3+}. The ΔG°_f of smectites also became less negative with increasing Fe^{3+} in the structure (Kudrat *et al.,* 2000). A database of ΔG°_f values for about 172 clay minerals is available in Varadachari *et al.* (2003).

(c) Phase diagrams

(i) Development of a method for deriving theoretical phase diagrams for clay mineral equilibria in aqueous systems

The method developed is based on the fact that at equilibrium, the free energy of a system is at minimum (Varadachari, 1992). Therefore, only that phase will be stable whose free energy of crystallization from solution (ΔG_c) is most negative amongst the ΔG_c values for all minerals. In this process, first every type of mineral that can be constituted from the component ions is considered. For each mineral, the ΔG_c value is computed. Minerals with positive ΔG_c are unstable phases. Amongst the minerals with negative ΔG_c values, the thermodynamically most stable phase is the one with the most negative value of ΔG_c. Since ΔG_c value changes with ionic conditions, each stable mineral will have certain boundary conditions of stability. Apart from thermodynamic factors, many phases with negative ΔG_c values may persist in the environment because of unfavourable kinetics resulting in metastable phases.

A phase diagram showing stable phases in the $\log[Si(OH)_4]$ and $\log[K^+/H^+]$ space with $\log[Mg^{2+}/(H^+)^2] = 9$, is shown in Fig. 2a. Under these conditions, kaolinite, muscovite and pyrophyllite are the only thermodynamically stable minerals. All other minerals such as biotite, phlogopite, talc, chlorite, microcline, smectites, clay micas, etc., are either unstable or metastable.

Table 5a. *Fuzzy membership grades and standard free energy data for some clay minerals*

Mineral	Membership (grades)			Standard free energy	
	Sample No.	$\mu^{illiite}$	μ^{Mica}	ΔG^0_f	ΔG^0_c
Illite	29	0.57	0.58	-1299.8	-7.96
	39	0.81	0.89	-1305.4	-10.45
	64	0.64	0.76	-1298.3	-11.54
	122	0.68	0.59	-1271.2	-11.23
	Centric	1.00	0.76	-1292.8	-10.01
		$\mu^{Glauconite}$	μ^{Mica}		
Glauconite	1	0.57	0.79	-1183.1	-10.98
	22	0.54	0.77	-1178.4	-7.75
	23	0.70	0.88	-1190.0	-6.02
	27	0.92	0.94	-1188.0	-3.15
	Centric	1.00	0.86	-1194.9	-3.96
		$\mu^{Celadonite}$	μ^{Mica}		
Celadonite	2	0.61	0.84	-1122.3	33.17
	9	0.55	0.84	-1144.1	31.34
	11	0.56	0.66	-1162.7	40.99
	16	0.63	0.93	-1163.2	33.71
	Centric	1.00	0.89	-1146.6	31.97
		$\mu^{Montmorillonite}$	$\mu^{Smecite}$		
Montmorillonite	1	0.60	0.80	-1264.8	-20.42
	2	0.70	0.82	-1267.7	-21.63
	3	0.58	0.73	-1275.8	-34.93
	4	0.52	0.85	-1269.0	-13.45
	9	0.61	0.80	-1272.9	-16.87
	Centric	1.00	0.91	-1262.6	-16.64
		$\mu^{Beidellite}$	$\mu^{Smecite}$		
Beidellite	8	0.52	0.73	-1283.9	-25.28
	10	0.52	0.83	-1292.4	-23.11
	Centric	1.00	0.96	-1294.3	-26.88
		$\mu^{Nontronite}$	$\mu^{Smecite}$		
Nontronite	42	0.57	0.69	-1133.1	-10.33
	Centric	1.00	0.96	-1119.8	-16.81
		$\mu^{Saponite}$	$\mu^{Smecite}$		
Saponite	3	0.72	0.81	-1335.3	49.43
	13	0.57	0.76	-1333.5	48.63
	14	0.72	0.78	-1336.4	48.32
	22	0.65	0.84	-1336.8	-17.84
	Centric	1.00	0.86	-1321.9	40.62
		$\mu^{Vermiculite}$	$\mu^{Vermiculite}$		
Vermiculite	17	0.73	0.99	-1298.0	120.09
	18	0.94	0.98	-1321.0	150.34
	33	0.61	0.53	-1364.8	144.80
	40	0.81	0.79	-1345.1	164.94
	Centric	1.00	1.00	-1319.7	146.09
Kaolinite		$\mu^{Kaolinite}$	$\mu^{Kaolinite}$		
	Centric	1.00	1.00	-912.1	-18.16

When the derivation is done after excluding the stable phases, mica and pyrophyllite, illite and montmorillonite appear (Fig. 2b). Illite appears in the muscovite region and montmorillonite appears in the pyrophyllite region; thus, illite is metastable with respect to muscovite and montmorillonite is metastable with respect to pyrophyllite.

Interestingly these derivations showed that the non-stoichiometric clay minerals like illite, montmorillonite, vermiculite, etc., are all metastable phases. Under normal ionic environments in soils, only the end members muscovite, pyrophyllite, talc, chlorite, phologopite and kaolinite are thermodynamically stable phases (Varadachari and Ghosh, 2003). The reason that non-stoichiometric clays persist in the environment is because the transformation process is impossible due to very high activation energies (kinetic barriers). Experimentally derived data points, when plotted in the theoretically derived phase diagrams, were found to lie well within the derived stability field for the corresponding end member (Varadachari and Ghosh, 2003). Thus, illites appear in the muscovite or phlogopite region and kaolinite appears in its own field. Experimental data show a good fit with the derived phase diagrams.

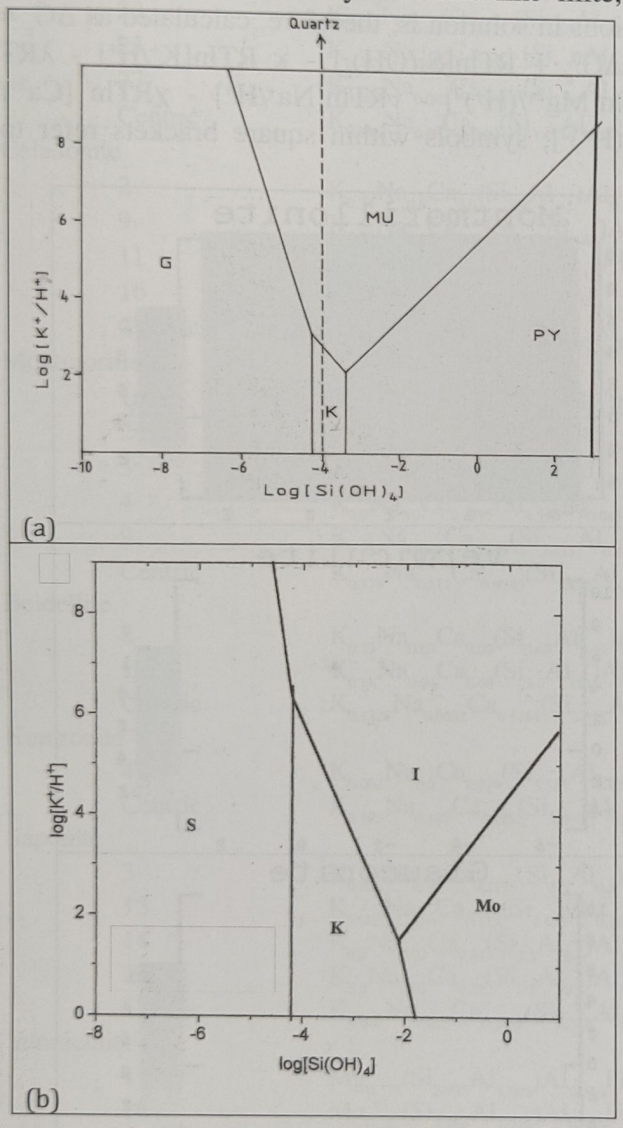

Fig. 2. *(a) Phase diagram at $log[Mg^{2+}/(H^+)^2] = 9$ showing stable phases and (b) metastable phases. K : kaolinite, Py : pyrophyllite, Mu : muscovite, Mo : montmorillonite, I : illite, S / G – solution with gibbsite, quartz, goethite phases.*

(ii) Fuzzy phase diagrams

Although the new methodology for derivation phase diagrams was a significant improvement over the earlier methodology, yet there was a need to get a better depiction of natural systems.

Particularly, phase diagrams could not depict multimineral assemblages or compositional variations and thereby could never provide a true representation of soils and sediments. There was a need to change the fundamental concepts which were based on conventional mathematics. Using the tools of fuzzy mathematics in thermodynamic derivations, Varadachari (2006) successfully incorporated the concept of graded, fuzzy transition zones of mineral transformation and multimineral occurrences.

Starting with a dataset of 464 clay mineral compositions, fuzzy membership values (grades) were derived. Those minerals with a grade ≥ 0.5 were chosen to ensure that only representative minerals were selected and those with compositional or classification errors were excluded (Varadachari, 2006). This generated a selective dataset of 170 clay minerals. Standard

free energies of formation, ΔG^0_f of all 170 minerals were derived as described earlier. Using the derived values of ΔG°_f, the standard free energy of crystallization from solution (ΔG^0_c) was evaluated (Varadachari 1992, 2006).

In a generalized equation, the ΔG^0_c for a mineral of composition $K_\kappa Na_\upsilon Ca_\chi Si_\sigma Al_\alpha Mg_\lambda Fe(III)_\Phi Fe(II)_\tau O_{10}(OH)_2$, is obtained from the reaction:

$$\lambda Mg^{2+} + \kappa K^+ + \chi Ca^{2+} + \upsilon Na+ + \Phi FeO(OH) + \tau FeO + \alpha Al(OH)_3 + \sigma Si(OH)_4 \Leftrightarrow$$

$$K_\kappa Na_\nu Ca_\chi Si_\sigma Al_\alpha Mg_\lambda Fe(III)_\Phi Fe(II)_\tau O_{10}(OH)_2 + (2\lambda + \kappa + 2\chi + \nu)H^+ + [\{(\Phi + 3\alpha + 4\sigma) - (2\lambda + \kappa + 2\chi + \nu + 2)\} \div 2]H_2O$$ (Varadachari, 2006).

Values of ΔG^0_c for some clay mineral compositions are shown in Table 5a along with their ΔG°_f values; compositions of these clay minerals are listed in Table 5b. Changing the concentrations of the ions in solution, changes the free energy of reaction; therefore, we need to estimate the free energy change for every ionic concentration. The free energy change of crystallization (ΔG_c) for a particular activity of ions in solution is, therefore, calculated as $\Delta G_c = \Delta G^0_c + RT\ln[Si(OH)_4] - \kappa\, RT\ln[K^+/H^+] - \lambda RT \ln[Mg^{2+}/(H^+)^2] - \nu RT\ln[Na^+/H^+] - \chi RT\ln [Ca^{2+}/(H^+)^2]$; symbols within square brackets refer to

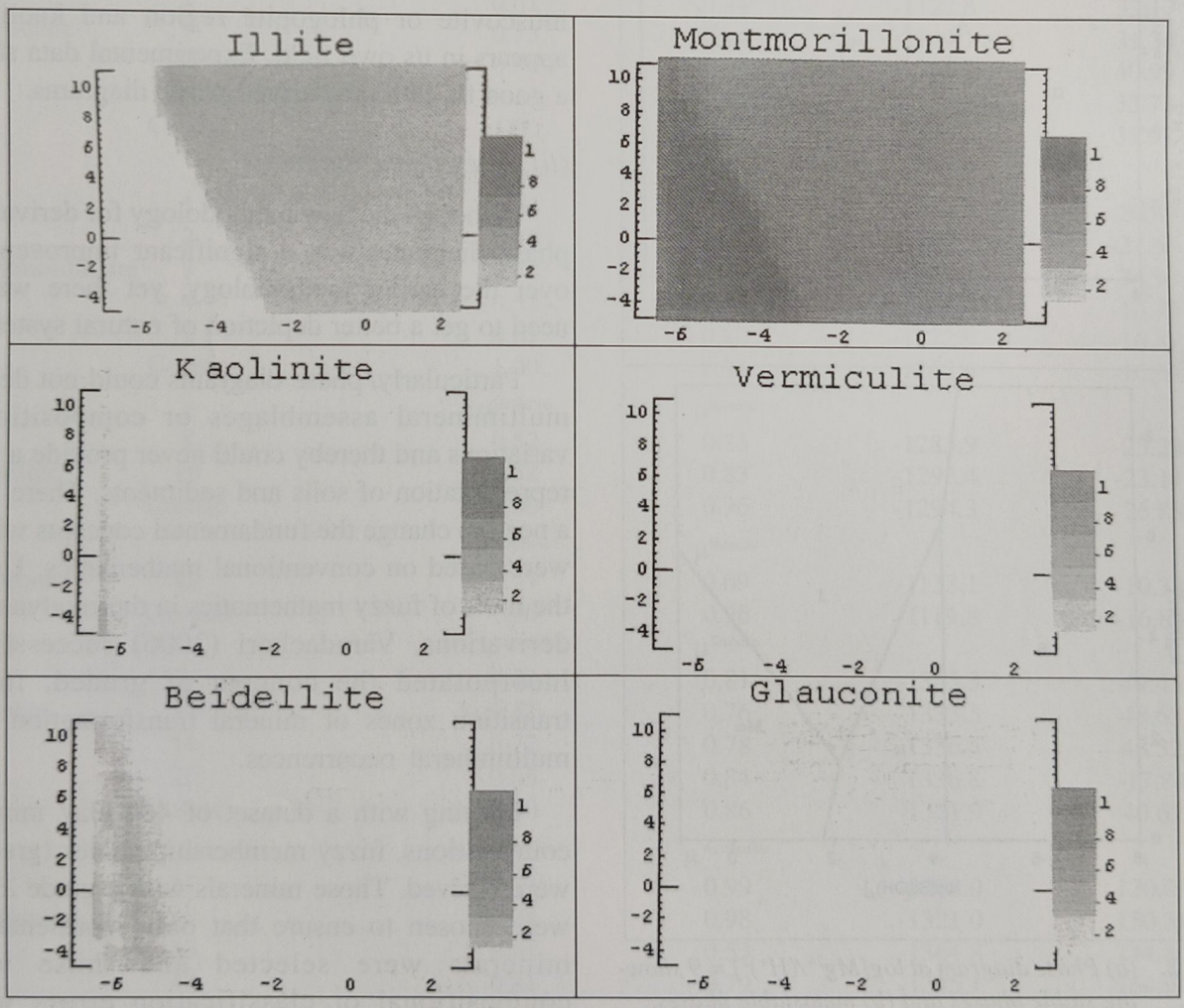

Fig. 3a. *2D fuzzy phase diagram showing grades of occurrence of clay minerals at $\log[Mg^{2+}/(H^+)^2] = 12$, $\log[Na^+/H^+] = 8$ and $\log[Ca^{2+}/(H^+)^2] = 6$; X-axis represents $\log[Si(OH)_4]$ and Y-axis represents $\log[K^+/H^+]$. Saponite, nontronite, celadonite and chlorite have zero grades under these conditions and are not represented here.*

Table 5b. *Compositions of clay minerals listed in Table 5a*

Illite (sample number)	Chemical composition of the clay minerals
29	$K_{0.56}Na_{0.04}(Si_{3.4}A_{l0.6})Al_{1.73}Fe^{III}_{0.03}Fe^{II}_{0.065}Mg_{0.295}O_{10}(OH)_2$
39	$K_{0.712}Na_{0.038}(Si_{3.44}Al_{0.56})Al_{1.74}Fe^{III}_{0.03}FeII_{0.02}Mg_{0.23}O_{10}(OH)_2$
64	$K_{0.642}Na_{0.038}(Si_{3.36}Al_{0.64})Al_{1.74}Fe^{III}_{0.12}Fe^{II}_{0.01}Mg_{0.18}O_{10}(OH)_2$
122	$K_{0.55}Na_{0.07}(Si_{3.51}Al_{0.49})Al_{1.54}FeIII_{0.29}Fe^{II}_{0.0}Mg_{0.19}O_{10}(OH)_2$
Centric	$K_{0.63}Na_{0.0624}(Si_{3.447}Al_{0.553})Al_{1.685}Fe^{III}_{0.1142}Fe^{II}_{0.0247}Mg_{0.2068}O_{10}(OH)_2$
Glauconite	
1	$K_{0.57}Na_{0.2}Ca_{0.03}\ (Si_{3.58}Al_{0.42})Al_{0.35}Fe^{III}_{1.12}Fe^{II}_{0.19}Mg_{0.4}O_{10}(OH)_2$
22	$K_{0.805}Na_{0.01}Ca_{0.025}\ (Si_{3.57}Al_{0.43})Al_{0.375}Fe^{III}_{1.15}Fe^{II}_{0.165}Mg_{0.33}O_{10}(OH)_2$
23	$K_{0.735}Na_{0.029}Ca_{0.045}\ (Si_{3.71}Al_{0.29})Al_{0.512}Fe^{III}_{0.99}Fe^{II}_{0.105}Mg_{0.36}O_{10}(OH)_2$
27	$K_{0.694}Na_{0.082}Ca_{0.037}\ (Si_{3.65}Al_{0.35})Al_{0.47}Fe^{III}_{0.97}Fe^{II}_{0.19}Mg_{0.4}O_{10}(OH)_2$
Centric	$K_{0.748}Na_{0.05}Ca_{0.03}(Si_{3.65}Al_{0.35})Al_{0.502}Fe^{III}_{0.95}Fe^{II}_{0.148}Mg_{0.42}O_{10}(OH)_2$
Celadonite	
2	$K_{0.73}Na_{0.0}Ca_{0.0}(Si_{3.9}Al_{0.1})Al_{0.08}Fe^{III}_{1.13}Fe^{II}_{0.25}Mg_{0.62}O_{10}(OH)_2$
9	$K_{0.73}Na_{0.0}Ca_{0.08}(Si_{3.78}Al_{0.22})Al_{0.2}Fe^{III}_{1.01}Fe^{II}_{0.28}Mg_{0.57}O_{10}(OH)_2$
11	$K_{0.84}Na_{0.01}Ca_{0.04}(Si_{3.9}Al_{0.1})Al_{0.36}Fe^{III}_{0.77}Fe^{II}_{0.21}Mg_{0.68}O_{10}(OH)_2$
16	$K_{0.72}Na_{0.045}Ca_{0.033}(Si_{3.87}Al_{0.13})Al_{0.338}Fe^{III}_{0.825}Fe^{II}_{0.21}Mg_{0.695}O_{10}(OH)_2$
Centric	$K_{0.701}Na_{0.0755}Ca_{0.052}(Si_{3.867}Al_{0.133})Al_{0.179}Fe^{III}_{1.0105}Fe^{II}_{0.196}Mg_{0.646}O_{10}(OH)_2$
Montmorillonite	
1	$K_{0.22}Na_{0.072}Ca_{0.051}(Si_{3.9}Al_{0.1})Al_{1.571}Fe^{III}_{0.14}Fe^{II}_{0.0525}Mg_{0.234}O_{10}(OH)_2$
2	$K_{0.22}Na_{0.0828}Ca_{0.053}(Si_{3.87}Al_{0.13})Al_{1.543}Fe^{III}_{0.186}Fe^{II}_{0.0051}Mg_{0.262}O_{10}(OH)_2$
3	$K_{0.17}Na_{0.056}Ca_{0.04}(Si_{3.884}Al_{0.116})Al_{1.579}Fe^{III}_{0.195}Fe^{II}_{0.0}Mg_{0.244}O_{10}(OH)_2$
4	$K_{0.0}Na_{0.0}Ca_{0.2175}(Si_{3.955}Al_{0.045})Al_{1.44}Fe^{III}_{0.105}Fe^{II}_{0.035}Mg_{0.4525}O_{10}(OH)_2$
9	$K_{0.25}Na_{0.083}Ca_{0.059}(Si_{3.853}Al_{0.147})Al_{1.4}Fe^{III}_{0.187}Fe^{II}_{0.0025}Mg_{0.465}O_{10}(OH)_2$
Centric	$K_{0.178}Na_{0.112}Ca_{0.0745}(Si_{3.823}Al_{0.177})Al_{1.453}Fe^{III}_{0.245}Fe^{II}_{0.0}Mg_{0.322}O_{10}(OH)_2$
Beidellite	
8	$K_{0.19}Na_{0.03}Ca_{0.05}(Si_{3.63}Al_{0.37})Al_{1.87}Fe^{III}_{0.1}Fe^{II}_{0.0}Mg_{0.07}O_{10}(OH)_2$
10	$K_{0.18}Na_{0.04}Ca_{0.08}(Si_{3.6}Al_{0.4})Al_{1.93}Fe^{III}_{0.03}Fe^{II}_{0.0}Mg_{0.07}O_{10}(OH)_2$
Centric	$K_{0.1328}Na_{0.0632}Ca_{0.1184}(Si_{3.625}Al_{0.375})Al_{1.86}Fe^{III}_{0.054}Fe^{II}_{0.0061}Mg_{0.094}O_{10}(OH)_2$
Nontronite	
42	$K_{0.062}Na_{0.0}Ca_{0.274}(Si_{3.525}Al_{0.475})Al_{0.0}Fe^{III}_{1.689}Fe^{II}_{0.0}Mg_{0.399}O_{10}(OH)_2$
Centric	$K_{0.105}Na_{0.107}Ca_{0.125}(Si_{3.592}Al_{0.408})Al_{0.052}Fe^{III}_{1.75}Fe^{II}_{0.0}Mg_{0.27}O_{10}(OH)_2$
Saponite	
3	$K_{0.025}Na_{0.04}Ca_{0.2175}(Si_{3.5}Al_{0.5})AlFe^{III}_{0.04}Fe^{II}_{0.0}Mg_{3.015}O_{10}(OH)_2$
13	$K_{0.005}Na_{0.0}Ca_{0.175}(Si_{3.615}Al_{0.385})Al_{0.0}Fe^{III}_{0.0}Fe^{II}_{0.0}Mg_{3.015}O_{10}(OH)_2$
14	$K_{0.0}Na_{0.02}Ca_{0.24}(Si_{3.5}Al_{0.5})Al_{0.02}Fe^{III}_{0.04}Fe^{II}_{0.0}Mg_{2.91}O_{10}(OH)_2$
22	$K_{0.0}Na_{0.02}Ca_{0.21}(Si_{3.5}Al_{0.5})Al_{0.04}Fe^{III}_{0.44}Fe^{II}_{0.0}Mg_{2.32}O_{10}(OH)_2$
Centric	$K_{0.017}Na_{0.027}Ca_{0.1895}(Si_{3.518}Al_{0.482})Al_{0.047}Fe^{III}_{0.083}Fe^{II}_{0.1105}Mg_{2.724}O_{10}(OH)_2$
Vermiculite	
17	$Mg_{0.375}(Si_{2.935}Al_{1.065})Al_{0.015}Fe^{III}_{0.51}Fe^{II}_{0.045}Mg_{2.325}O_{10}(OH)_2$
18	$Mg_{0.367}(Si_{2.785}Al_{1.215})Al_{0.097}Fe^{III}_{0.39}Fe^{II}_{0.03}Mg_{2.48}O_{10}(OH)_2$
33	$Mg_{0.5}(Si_{2.86}Al_{1.14})Al_{0.15}Fe^{III}_{0.01}Fe^{II}_{0.0}Mg_{2.83}O_{10}(OH)_2$
40	$Mg_{0.43}(Si_{2.72}Al_{1.28})Al_{0.017}Fe^{III}Fe^{II}_{0.14}Mg_{2.62}O_{10}(OH)_2$
Centric	$Mg_{0.373}(Si_{2.81}Al_{1.19})Al_{0.086}Fe^{III}_{0.408}\ Fe^{II}_{0.0}Mg_{2.481}O_{10}(OH)_2$
Kaolinite	
Centric	$Si_2Al_2O_5(OH)_4$

activities in moles/L (Varadachari, 2006). In the construction of a 2D phase diagram (a biaxial graph), only two ionic components can be considered as variables. The other ionic components have to be assigned some constant values. A diagram that is constructed in a

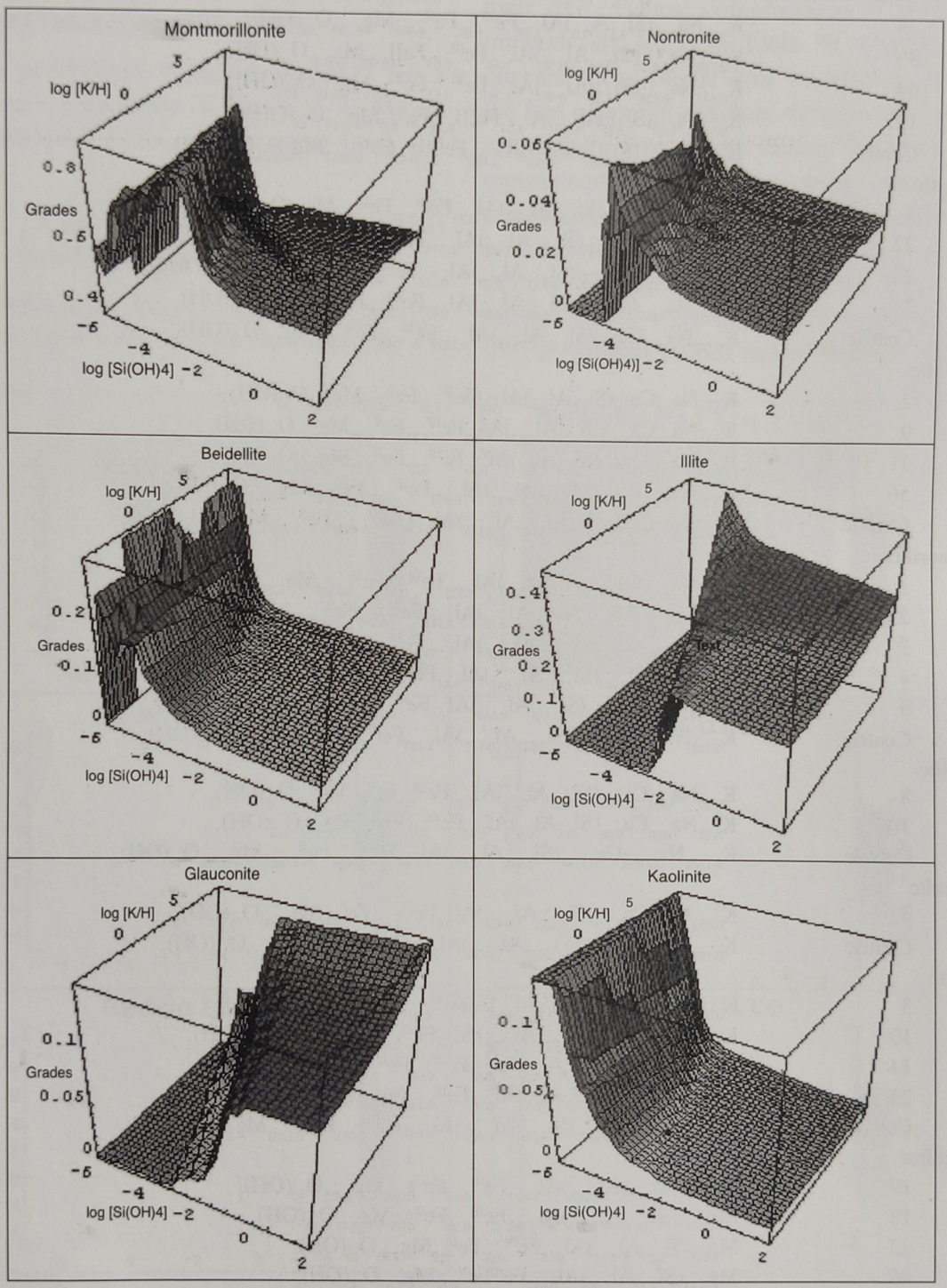

Fig. 3b. *3D fuzzy phase diagram of clay minerals showing grades of occurrence along z-axis at* $\log[Mg^{2+}/(H^+)^2] = 9$, $\log[Na^+/H^+] = 6$ *and* $\log[Ca^{2+}/(H^+)^2] = 9$. *Saponite, celadonite, vermiculite and chlorite have zero grades under these conditions and are not represented here*

$\log[Si(OH)_4]$ - $\log[K^+/H^+]$ axis has constant values of $\log[Mg^{2+}/(H^+)^2]$, $\log[Na^+/H^+]$ and $\log[Ca^{2+}/(H^+)^2]$. Then ΔG_c is evaluated for values of $\log[Si(OH)_4]$ and $\log[K^+/H^+]$ at small interval increments for each of the 170 minerals. Then the ΔG_c of every mineral is compared with the ΔG_c of all minerals in other groups. In these comparisons, the mineral having the more negative value of ΔG_c is considered more stable and is assigned a weightage of 1. The density of occurrence of a mineral relative to total occurrences is then computed on a scale of 1 to 0. The computation is repeated over the entire range of $\log[Si(OH)_4]$ and $\log[K^+/H^+]$ values. The data (in fractional numbers) represent the grade of mineral occurrences.

Results of fuzzy phase diagrams under various conditions of pH and cationic activities show how different minerals dominate in different environments. Thus, at low pH and low activities

Chemical composition (as weight % Al_2O_3 / SiO_2 / K_2O / M_xO_y, etc.)

↓

Convert to gram equivalent for all cations, e.g., (wt% of Al_2O_3 × valency of Al × no. of atoms of Al in Al_2O_3) ÷(mol wt of oxide, Al_2O_3) = (wt% of Al_2O_3 × 6) ÷ 101.961

↓

Add g eq for all cations
[Total g eq all cations = g eq of Al + g eq of Si + g eq of Fe^{III} + g eq of K + .. etc]

↓

Convert to g eq for a half unit cell having 22 anionic charges due to $O_{10}(OH)_2$
[e.g., (g eq of Al × 22) ÷(total g eq of all cations)]

↓

Obtain atoms per half unit cell by dividing by valency
[e.g., g eq Al for half unit cell ÷ 3]

↓

Check for charge neutrality by adding total cationic charge in half unit cell; this should be 22; if there is minor deviation adjust amounts of interlayer cations so that total cationic charge is exactly 22.

↓

Calculate tetrahedral charge (TC) as 4 – Si in half cell [if Si = 3.7 then TC = 4-3.7 = 0.3]

↓

Tetrahedral Al (^{IV}Al) is the same as the TC [thus ^{IV}Al = 0.3]

↓

Octahedral charge (OC) is by multiplying octahedral cations by their valency and subtracting 6 from it; 6 being the anionic charge in octahedral layer

↓

Total layer charge (TLC) is the sum of TC and OC [TLC = TC + OC]

↓

Broad group classification obtained by deriving classification scores from the formulae for the 3 broad groups, viz., clay mica (P_{CM}), smectite (P_S), vermiculite (P_V)
(Formulae in Table 1) using x= TLC, y = K in half unit cell
The mineral belongs to the group which has the highest score

↓

Subgroup classification obtained by deriving classification scores from the formulae for the 7 subgroups, viz., illite (S_i), glauconite (S_g), celadonite (S_c), montmorillonite (S_m), nontronite (S_n), beidellite (S_b), saponite (S_s) using formulae in Table 2
The mineral belongs to the group which has the highest score

Fig. 4a. *Flowchart showing the steps in deriving clay mineral classification at group, subgroup and grade level starting from composition*

of Mg^{2+}, Na^+ and Ca^{2+}, such as $\log[Mg^{2+}/(H^+)^2] = -2$, $\log[Na^+/H^+] = -4$, $\log[Ca^{2+}/(H^+)^2] = -2$, kaolinite shows up as the dominant phase with a grade of 0.6 at $\log[Si(OH)_4] < -5$. As silica activity increases to $\log[Si(OH)_4] > -4$, montmorillonite appears in significant proportions (Varadachari, 2006). At near neutral pH and higher activities of Mg^{2+}, Na^+ and Ca^{2+}, such as $\log[Mg^{2+}/(H^+)^2] = 7$, $\log[Na^+/H^+] = 3$, $\log[Ca^{2+}/(H^+)^2] = 7$, montmorillonite dominates at $\log[Si(OH)_4] \sim -3$ with a zonal grade of around 0.8. The high K^+ activity zones show illitic regions with grades around 0.4. At high pH and high levels of Mg^{2+}, Na^+ and Ca^{2+}, montmorillonite predominates with associated beidellite and saponite (Varadachari, 2006).

Fig. 3a is an example of a 2D fuzzy phase diagram in a $\log[Si(OH)_4]$ and $\log[K^+/H^+]$ space with $\log[Mg^{2+}/(H^+)^2] = 12$, $\log[Na^+/H^+] = 8$ and $\log[Ca^{2+}/(H^+)^2] = 6$. These conditions (of Mg^{2+}, Na^+, Ca^{2+} and H^+) represent high pH and cation activity levels. Zonal grades or intensities of occurrences are represented by the shades of grey. Thus, illite has negligible occurrence at $\log[Si(OH)_4] = -4$ and $\log[K^+/H^+] = -2$; however, in the same region, zonal grade for montmorillonite is around 0.8. The only other mineral with some presence in this region is beidellite. Phase diagrams can also be represented as a 3D map with the zonal grade of the mineral in the z-axis. Fig. 3b is an example of a 3D diagram in $\log[Si(OH)_4]$ - $\log[K^+/H^+]$ space with $\log[Mg^{2+}/(H^+)^2] = 9$, $\log[Na^+/H^+] = 6$ and $\log[Ca^{2+}/(H^+)^2] = 9$. In this graph, the zonal grades of the minerals can be directly read. Zonal grades for vermiculite, chlorite and celadonite are negligible whereas zonal grade for montmorillonite peaks at about 0.8, for illite at 0.4 and for beidellite at 0.2.

Derived phase diagrams show good fit with experimental observations from compositions of aqueous systems in equilibrium with minerals. Some of the examples are cited here. Stream waters analysed by Norton (1974) are predicted to have mineralogy of montmorillonite (grade 0.7) and kaolinite (grade 0.1); the observed mineralogy is predominantly montmorillonite with associated kaolinite. Similarly, the water

Calculate fuzzy membership grade for broad group parameters, TLC & K using formulae $\mu_{\alpha_i}{}^G(s) = 1 - \{|\alpha_i(s) - \alpha_i{}^G{}_{centric}| / \Gamma\}$ where $\alpha_i(s)$ is a value of a parameter, i, (e.g., TLC) of a sample s in some mineral broad group G (e.g., smectite) having a database of r samples, $\alpha_i{}^G{}_{centric}$ is the centric or typical value of the parameter α_i for the group G; thereby, $|\alpha_i(s) - \alpha_i{}^G{}_{centric}|$ represents the Euclidean distance of $\alpha_i(s)$ from $\alpha_i{}^G{}_{centric}$ and Γ is the maximum observed distance from the centric value, of the α_i parameter, in the mineral group/subgroup G ($\alpha_i{}^G{}_{centric}$ and Γ values available in Mukherjee et al 2006)

↓

Combine the individual membership values of both parameters (TLC & K) using the equation $\mu_{\alpha_1,\alpha_2}{}^G = t(\mu_{\alpha_1}{}^G, \mu_{\alpha_2}{}^G) = \mu_{\alpha_1}{}^G \times \mu_{\alpha_2}{}^G / [(\mu_{\alpha_1}{}^G)^{0.5} + (\mu_{\alpha_2}{}^G)^{0.5} - (\mu_{\alpha_1}{}^G \times \mu_{\alpha_2}{}^G)^{0.5}]^{1/0.5}$

↓

Calculate fuzzy membership grade for subgroup parameters, Al (VI), Mg (VI), OC and TC using the same process as for broad groups

↓

Combine the grades of subgroup parameters as shown for broad group. Aggregate the grades taking any two of them and aggregating the result with the third, then subsequently with the fourth.

↓

The resulting value shows the belongingness of a mineral to that subgroup. Minerals having grades <0.5 should not be taken for further derivations because they are not sufficiently representative of that group.

Fig. 4b. *Flowchart showing the steps in deriving clay mineral classification at grade level (fuzzy membership value)*

analysis of a spring in Lake Chad, which is montmorillonitic (Tardy, 1971), is predicted to have a montmorillonite zone of grade 0.8. Another sample from Lake Chad with montmorillonite-beidellite assemblage (Tardy, 1971) is predicted from the diagrams to have composition of montmorillonite-beidellite of grade 0.6 (Varadachari, 2006).

Conclusion

Some interesting deductions from the phase diagrams are that (a) illite occurrences are always associated with montmorillonite, (b) however, montmorillonite occurrences can occur without illite as a co-phase, (c) surface neoformation processes will only produce admixtures; occurrences of pure clay mineral phases are very rare, (d) montmorillonite can occur in greatest abundance in the inorganic phase in soils, (e) kaolinite is the only other mineral that could dominate the soil mineralogy, (f) illite, beidellite, vermiculite occur only in association and never as the dominant phase, (g) saponite, celadonite can be present only as a rare occurrence.

This is for the first time, the phase diagrams show a fairly good fit with experimental observations. Also for the first time, a method is available that allows us to predict multimineral assemblages. The predictions are not limited to the nature of the minerals but also the intensity of their occurrences. It explains some interesting facts such as why nature produces highly montmorillonitic or kaolinitic soils (black soils or laterites) but there is no other soil whose mineral matrix is equally dominant with respect to other clay minerals like illite, glauconite or vermiculite.

Further derivations of more phase diagrams under more diverse environmental conditions, could reveal more such interesting facts about clay minerals and their occurrences in soils and aquatic environments.

Finally, fuzzy phase diagram is a strikingly novel proposition not just restricted to clay mineralogy but to physical chemistry itself. This concept could always be extended to variable composition complex mineralogical and metallurgical systems.

References

Chen, C. 1975. A method of estimation of standard free energies of formation of silicate minerals at 298.15 K. *Am. J. Sci.* **275** : 801-817.

Garrels, R.M. and Christ, C.L. 1965. *Solutions, Minerals and Equilibria.* Harper & Row, New York.

Helgeson, H.C., Brown, T.H. and Leeper, R.H. 1969. *Handbook of Theoretical Activity Diagrams Depicting Chemical Equilibria in Geologic Systems Involving an Aqueous Phase at One Atm and 0° to 300°C.* Freeman Cooper, San Francisco.

Karpov, I.K. and Kashik, S.A. 1968. Computer calculation of standard isobaric-isothermal potentials of silicates by suitable regression from crystallochemical classifcation. *Geochem. Int.* **6** : 706-713.

Kudrat, M., Sharma, K.P., Varadachari, C. and Ghosh, K. 1999. An algorithm and program in C language for computation of standard free energy of formation of clay minerals. *Comp. Geosci.* **25** : 241-250.

Kudrat, M., Varadachari, C. and Ghosh, K. 2000. Application of the improved regression method to derive ΔG°_{f} of non-stoichiometric clay minerals and their correlations with compositional parameters. *Chem. Geol.* **168**: 225-238.

Mukherjee, G., Varadachari, C. and Ghosh, K. 2006a. Identification of 2 : 1 clay minerals from compositional data. *Clay Res.* **25** : 105-116.

Mukherjee, G., Varadachari, C. and Ghosh, K. 2006b. Grading clay minerals. *Clay Res.* **25:** 129-140.

Newman, A.C.D. 1987. *Chemistry of Clays and Clay Minerals*. Wiley-Interscience, New York.

Norton, D. 1974. Chemical mass transfer in the Rio Tanama system, West-Central Puerto Rico. *Geochim. Cosmochim. Acta* **38** : 2657-2677.

Nriagu, J.O. 1975. Thermochemical approximations for clay minerals. *Am. Miner.* **60** : 834-839.

Slaughter, M. 1966. Chemical bonding in the silicate minerals. Part I. Model for determining crystalchemical properties. *Geochim. Cosmochim. Acta* **30** : 299-313.

Sposito, G. 1986. The polymer model of thermochemical clay mineral stability. *Clays Clay Miner.* **34** : 198-203.

Tardy, Y. 1971. Characterisation of the principal weathering types by the geochemistry of waters from some European and African crystalline massifs. *Chem. Geol.* **7** : 253-271.

Tardy, Y. and Duplay, J. 1994. Stability fields of smectites and illites including glauconites as a function of temperature and chemical composition. In (K.H. Wolf and G.V. Chilingarian, Ed.), *Developments in Sedimentology. 51. Diagenesis IV*. Elsevier, Amsterdam, pp. 95-132.

Tardy, Y. and Garrels, R.M. 1974. A method of estimating the Gibbs energies of formation of layer silicates. *Geochim. Cosmochim. Acta* **38** : 1101-1116.

Tardy, Y. and Garrels, R.M. 1977. Prediction of Gibbs energies of formation of compound from the elements. II. Monovalent and divalent metal silicates. *Geochim. Cosmochim. Acta* **41** : 81-92.

Varadachari, C. 1992. Constructing phase diagrams for silicate minerals in equilibrium with an aqueous phase : A theoretical approach. *Soil Sci.* **153** : 5-12.

Varadachari, C. 2006. Fuzzy phase diagrams of clay minerals. *Clays Clay Miner.* **54** : 616-625.

Varadachari, C. and Ghosh, K. 2003. Thermodynamic derivation of new low temperature phase diagrams for phyllosilicates defining stable and metastable phases. *Indian J. Geol.* **75 :** 203-217.

Varadachari, C. and Ghosh, K. 2009. Use of statistics in assigning fuzzy membership values to clay minerals of variable composition. *Clay Res.* **28** :1-5.

Varadachari, C. and Mukherjee, G. 2004. Discriminant analysis of clay mineral compositions. *Clays Clay Miner.* **52 :** 311-320.

Varadachari C., Kudrat M. and Ghosh K. 1994. Evaluation of standard free energies of formation of clay minerals by an improved regression method. *Clays Clay Miner.* **42** : 298-307.

Varadachari, C., Mukherjee, G., Goswami, D. P. and Chakraborty, M. K. 2003. Understanding clay minerals with fuzzy mathematics. *Naturwissenschaften* **90** : 44-48.

(Received November 2017 accepted December 2017)

About the Speaker

Dr Chandrika Varadachari was born in Tiruchirapalli, Tamil Nadu in a distinguished Thanjvur Iyengar family of Shrirangam.

Dr Chandrika had her schooling at St Mary's School, Tiruchirapalli, St Agnes Convent, Howrah and St Mary's School, Gauhati. Later she studied at Lady Brabourne College, Kolkata and Calcutta University for her BSc (Chemistry Hons), MSc and PhD in Agricultural Chemistry and Soil Science. She is a recipient of Calcutta University Gold Medal and AC Sen Memorial Gold Medal of Calcutta University.

In 1986, Dr Chandrika received the *Young Scientist Award* of the Indian National Science Academy (INSA), highest recognition of talent for a Young Scientist in India. She was the first recipient from Soil Science or Agricultural Chemistry or Agricultural Chemicals and the youngest awardee of that year. Later in 1988, she was awarded *Young Scientist Award* of the Department of Science & Technology (DST), Government of India.

In recognition of her seminal work on fertilizer development, *UNESCO-ROSTCA Award* in Chemistry was conferred on her in 1990. In 2008, she was awarded *Lockheed-Martin India Innovation Award* for technology of highest commercial potential out of 362 technologies submitted by Government Departments/Councils, Universities, Research Institutes, IITs and private sector. The assessment was done globally by the IC2 Institute, University of Texas at Austin in collaboration with FICCI, New Delhi and DST, Government of India.

Dr Chandrika is a Fellow and currently Council Member of the National Academy of Agricultural Sciences (NAAS) and also a Fellow of the West Bengal Academy of Science & Technology (WAST).

The research interests of Dr Chandrika are diverse. They include fertilizer technology, analytical methods, soil physical chemistry, soil environmental chemistry, clay mineralogy, soil organic matter, organic agriculture to even hard core physical chemistry and computational material science. She is also one of the leading experts in Patents and IPR.

Interestingly, the last two Review Articles by late Professor SK Mukherjee are incidentally the first two Review Articles of Dr Chandrika being co-author, one for the Bulletin of the Indian Society of Soil Science and the other for Clay Research, both on Clay Mineralogy.

At present, Dr Chandrika is the Director of Raman Centre for Applied and Interdisciplinary Sciences, Kolkata and President & CTO of Agtec Innovations Inc, Los Altos, California.

About the Lecture

While organising the 17th Annual Convention, an appeal for fund was made to various academia in Kolkata to honour the memory of late Professor SK Mukherjee, Founder President of CMSI. As a result, "Professor SK Mukherjee – Clay Minerals Society of India Foundation Lecture" was instituted and the first lecture entitled "Clay Mineral Structures : The Beauty of Symmetry and the Enigma of Quasicrystals" was delivered by Professor Kunal Ghosh, University of Calcutta, Kolkata on 27 April 2012 during the 17th Annual Convention in Kolkata. The second lecture was on "Soil Modifiers : Their Advantages and Challenges" and the speaker was Dr DK Pal, NBSS & LUP, Nagpur; it was arranged on 27 September 2013 during the 18th Annual Convention in New Delhi. Dr SC Datta, IARI, New Delhi in the third lecture during the 19th Annual Convention in Kolkata on 7 August 2015, spoke on "Molecular Orientation in Mica and its Implication on Potassium Fertility of Soil". The fourth lecture entitled "Clay Mineral Equilibria : Fuzzy Phase Diagrams" was delivered by Dr Chandrika Varadachari, RCAIS, Kolkata on 17 February 2017 during the 20th Annual Convention in Nagpur.

Clay Research, Vol. 36, No. 1, pp. 17-22 (2017)

Natural Dye Intercalated Clay Hybrid Material: Clay based Nanopigment

T. CHOUDHURY*

Department of Chemistry, School of Advanced Sciences, Vellore Institute of Technology, Chennai

Abstract–*Natural dye (Turmeric) was intercalated into montmorillonite by ion exchange and adsorption processes in an attempt to improve the colour fastness and fading property of the dye and also to study the thermal characteristics of the hybrid material thus prepared for wall plastering applications. The resulting nano pigment was characterized by X-ray Diffractometer (XRD), Fourier Transform Infra Red Spectroscopy (FTIR), and Thermal Gravimetric Analysis (TGA). XRD results confirmed an increase in d spacing of 3.5 Å for nanopigment as compared to pure montmorillonite. TGA revealed an increase in thermal stabilities of all samples and also showed delayed decomposition for sample S4 in which clay content was higher, thus ascertaining the effect of barrier property of clay. FTIR results established the bond formation between turmeric and montmorillonite. Thus all results indicate that intercalation of dye into montmorillonite has taken place successfully.*

Key words : Montmorillonite, Natural Yellow, Adsorption, Nanopigment, TGA, FTIR, XRD

[1]Introduction

Clays are widely applied in many fields such as polymer nano-composites (Sinha Ray S 2003, Fischer H 2003, Zheng Q *et al.,* 2005), adsorbents for heavy metal ions (Bradl H B., 2004), catalysts (Gil A *et al.,* 2000), photochemical reaction fields (Shichi T., 2000), ceramics (Burst J F., 1991), paper filling and coating (Bundy W H., 1991), sensors and biosensors (Mousty C., 2004), due to their high specific surface area, chemical and mechanical stabilities, and a variety of surface and structural property (Murray H H 1991., 2000). In recent years, clay has been accepted as one of the low cost adsorbents for the removal of dyes. Among the studied clays, expandable layered silicates as adsorbents have received considerable recognition (Rytwo G *et al.,* 2000, Gemeay A H *et al.,* 2002, Holzheu S *et al.,* 2002; Wang C C *et al.,* 2004)

Dyes are flat polyaromatic molecules that bind selectively to the clay surface over a wide pH range. They are generally cationic due to the presence of amino groups, e. g 9-aminoacridine (9-Aa), 3, 6-diaminoacridine (3, 6 Daa), azure A (Az-A) and safranin O (Saf-O). It has been suggested that dyes are generally hydrophobic in nature and generally adsorb in aggregates at the flat silica faces of clay mineral which is made hydrophobic by cation exchange process, to give rise to organo montmorillonite (OMt). It is due to their nanostructured morphology that these OMts are called nanopigments. Many works have been carried out in quantitative aspects and model the adsorption behavior of the dye molecules to the clay surface. (Harris R G *et al.,* 2006)

Rhodamine was intercalated at 100% of the cationic exchange capacity of montmorillonite to produce clay hybrid nanopigments and nanopigment/ PP nanocomposites with improved

***Corresponding Author Email :** tanushree.c@vit.ac.in

photostability (Raha S *et al.*, 2009). More recently, chemically modified non ionic dyes were ionic exchanged with Na^+- MMT and fixed with PP, obtaining a reduction in the migration of the dye (Raha S *et al.*, 2012). Several blue nanopigments were prepared by exchanging methylene blue (MB) and a Na^+- MMT (OMt-MB) (Beltran M I *et al.*, 2014). The photolysis of rhodamine 6 G, a cationic xanthenes dye was studied by immobilizing it in layered hexaniobates (Shinozaki R., 2008).

There have been many reports in literature in the past decade over the use of synthetic dyes in textile industry due to their ease in availability and excellent colour fastness properties. The use of natural dyes is slowly gaining momentum due to increase in awareness of environmental and health hazards that are associated with synthesis, processing and use of synthetic dyes. The only major drawback that restricts the potential application of natural dyes is its poor fastness to light and ozone (Baez E., 2008). Nano composite pigment based on inorganic/organic interactions is an alternative for enhancing the UV resistance and fastness of dye based colourants.

Out of many natural dyes available, the current work deals with the encapsulation of Natural Yellow or turmeric dye onto montmorillonite clay mineral. Turmeric (Curcumin longa) is a plant native to South India and Indonesia, and is also cultivated in China and the whole of South East Asia (Umbreem S., 2008). Curcumin {(1E, 6E) - 1, 7-bis (4-hydroxy-3-methoxy phenyl)-1, 6- heptadiene-3, 5- dione} also known as Natural Yellow, is a hydrophobic polyphenolic compound, obtained from the dried rhizomes of Curcuma longa (Dutta A., 2013). Curcumin is a non ionic dye which exists in keto enol tautomerism with equilibrium strongly favouring an enol form as shown in figure 1. The enol structure enables curcumin to form additional inter and intramolecular H-bonds (El-Shishtawy R M., 2009).


Turmeric Plant with Rhizome

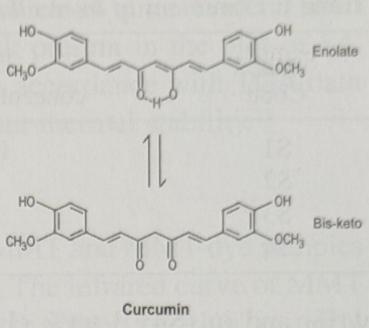

Curcumin

Fig. 1. *Structure of Curcumin (Natural Yellow) Dye*

The objective of the present paper is to attain an applicable method in preparation of natural dye intercalated montmorillonite suitable for wall plastering and in textile industry. In this manner, intercalation of natural dye in MMt was done through an adsorption process in different reaction conditions. The effect of intercalation of dye into MMT on its interlayer spacing was investigated using X-ray diffraction technique. The utilization of the nanopigment for further applications like 'wall plastering' demands thermal characterization. Colour fastness of the material was studied as a function of TGA, because if the stability of the dye in host is higher, the colour fading will also be reduced (Joseph L K., 2009). Bonding between clay and dye was studied by FTIR.

Materials and Methods

Materials: Clay used in this experiment was Montmorillonite KSF from Aldrich Chemicals, India. Cetyl trimethyl ammonium bromide (CTAB) used for dispersing clay was acquired from SD-Fine Chemicals, India. Natural Yellow dye used as an intercalant was obtained from natural source, India.

Preparation of Organo-Montmorillonite (O-Mt) Nanopigment

Natural Yellow intercalation into montmorillonite was done at different conditions as quoted in Table 1. In samples (S1- S3), 1

Table 1. *Conditions of Intercalation processes*

Sample Code	Dye concentration (g)	Intercalation time (Hrs)	Concentration of Clay suspension (wt %)
S1	0.5	3	1
S2	1	3	1
S3	5	3	1
S4	3	3	3

wt%, and in (S4) 3 wt% clay suspensions were first prepared under mechanical stirring in deionized water for three hours. The suspensions were made organophilic by adding 1wt% cetyl trimethyl ammoniumbromide (CTAB) to all samples. Then a predissolved amount of dye ranging from 0.5 to 1.5 times of cation exchange capacity (CEC) of montmorillonite was slowly added to the clay suspensions at room temperature and the reaction mixture was stirred for three hours. At the end of the process, the coloured hybrid products were separated from liquid phase by centrifugation for 30 minutes at 4000 rpm. The products were washed with deionized water repeatedly to remove any excess dye. After drying at room temperature, the intercalation products were ground using mortar.

Results and Discussions

TGA Analysis

TGA curves for natural turmeric dye (S5), and natural dye intercalated MMT samples containing 1 wt% and 3 wt% organo clay for samples S1 to S4 are shown in Figure 2. Natural Yellow turmeric dye curve shows a sharp peak with a maximum at 35.7^{0}C. For the same proportion of organo clay (1wt%), nanopigments containing montmorillonite (S1, S2, S3) decompose at a higher temperature than natural yellow turmeric dye (S5) as is evident in the TGA plot. S4, containing 3 wt% organo clay shows second decomposition peak in DTGA plot at 450^{0}C. This shoulder is very much reduced and resembles a broad hump in the figure as compared to other samples (S1, S2, and S3). This decomposition is delayed because of increase in content of clay (3wt %) which has a barrier effect on the diffusion of volatile compounds (Corres M A et al., 2013). These results thus indicate that thermal stabilities of MMT-dye samples are higher than pure natural yellow dye due to intercalation of dye into clay galleries.

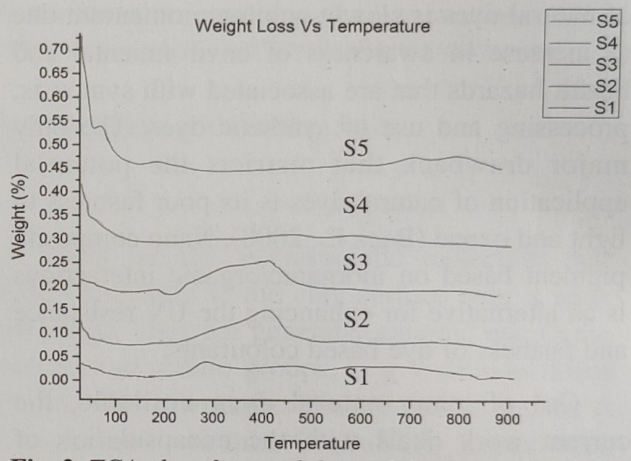

Fig. 2. *TGA plot of natural dye and dye intercalated clay hybrids*

XRD Analysis

Figure 3 shows the XRD patterns of MMT and the prepared MMT-Natural Yellow dye samples with different concentrations of dye and MMT. As it can be seen, samples S2 and S3 show broadening and shifting of peak to lower angles (2θ= 5.72) and (2θ= 5.35) respectively. This observed shift implies to the increase in the respective basal spacing from 13.00 A^0 for the untreated MMT to more expanded basal spacing, which could be attributed to the intercalation of dye molecules into the interlayer spaces of MMT. As the dye concentration increases in samples

(S1, S2, and S3), basal spacing also increases accordingly. Therefore, larger distances between the clay galleries were achieved in the intercalation processes with concentrated dye solution. This may be due to the fact that highly concentrated solutions of dye contain higher agglomeration which leads to more adsorption of dye on MMT and consequently higher basal spacing. But this is not true for sample S4 which shows marginal increase in d-spacing (d= 13.58A^0) for clay concentration 3 wt%. This may be due to the presence of higher concentration of clay in the sample which is quite evident from the sharp intense peak present in the plot of S4. This observance is in accordance with TGA data where S4 shows higher thermal stability.

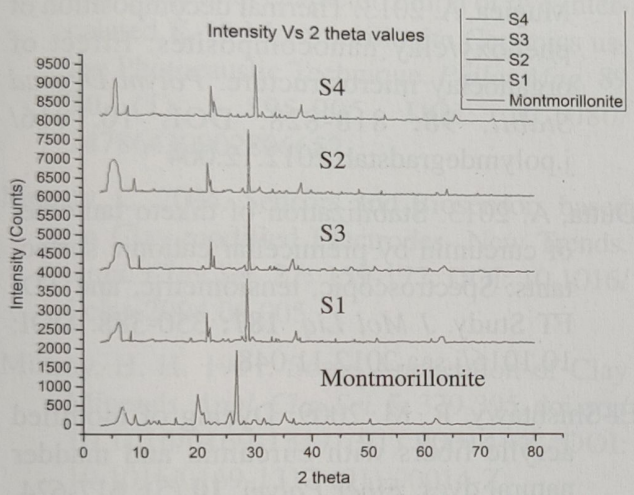

Fig. 3. *XRD of Montmorillonite and dye intercalated Montmorillonite samples*

FTIR Analysis

FTIR spectra of MMT and MMT-dye samples are shown in figure 4. The infrared curve of MMT showed characteristic smectite clay mineral peaks.

The peak at 1642.17 cm^{-1}, and broad band at 3439.76 cm^{-1} were assigned to O-H bending and stretching vibration modes of adsorbed water respectively. Also the peak at 3629.83 cm^{-1} corresponds to the structural hydroxyl stretching vibration bonded to Al/Mg in MMT. These peaks appeared in the spectrum of MMT-dye samples.

The bands at 2924.71 cm^{-1} and 2865.63 cm^{-1} corresponded to the asymmetric and symmetric vibration of C-H bonds in $-CH_2$ group of MMT. Strong band at 1041 cm^{-1} was attributed to Si-O-Si asymmetric stretch vibration for MMT which was greatly reduced in intensity for MMT-dye peak. This indicates the existence of Natural Yellow dye as an intercalant in exchanged products which is in accordance to results obtained from XRD.

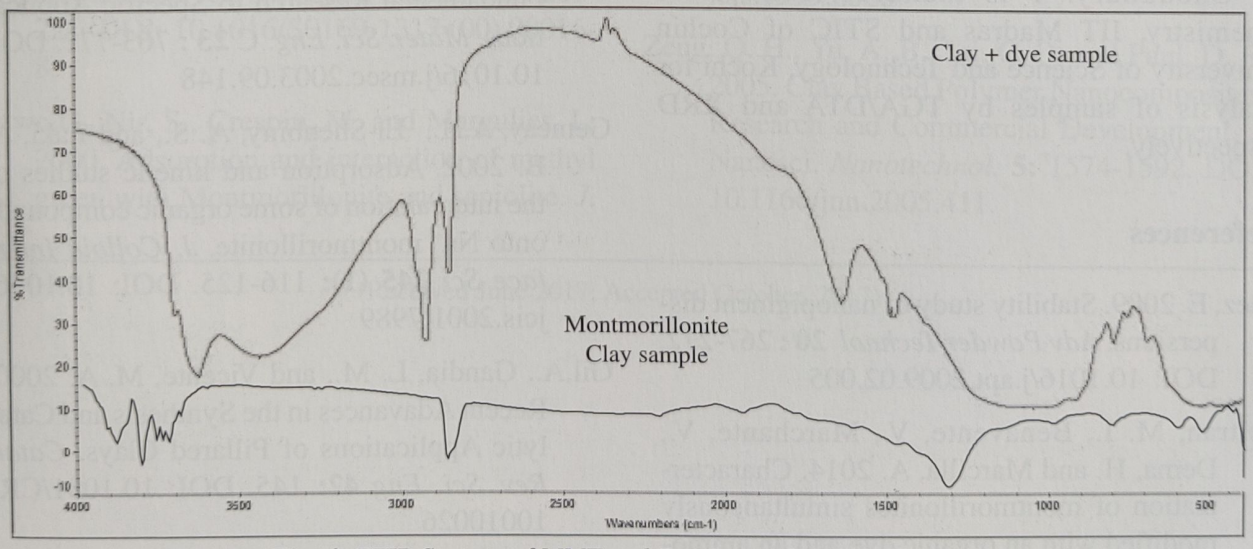

Fig. 4. *FTIR Spectra of MMT and Dye Intercalated MMT sample*

Conclusion

The present study deals with the intercalation of natural dye into montmorillonite under different conditions of dye and clay concentrations and process time.

Results obtained from XRD confirmed the process of intercalation of dye into MMT. The highest d-spacing value being recorded for MMT-dye sample is 16.496 Å, thus confirming that interlayer space increased with dye concentration. But these results are in stark contrast to sample S4 which showed sharp intense peak due to the presence of higher concentration of clay in it. The intercalation process was also confirmed by FTIR. TGA/DTA thermograms showed that the thermal stabilities of natural dye molecules between interlayers of MMT increase considerably as compared to pure dye.

By investigating above important parameters on intercalation of Natural Yellow into MMT layers, a nano pigment has been formed which can be used for wall plastering applications and its potential in coloration remains a target for future work.

Acknowledgement

Choudhury. T is thankful to Dept. of Chemistry, IIT Madras and STIC of Cochin University of Science and Technology, Kochi for analysis of samples by TGA/DTA and XRD respectively.

References

Baez, E. 2009. Stability study of nanopigment dispersions. *Adv Powder Technol* **20 :** 267-272. DOI: 10.1016/j.apt.2009.02.005

Beltran, M. I., Benavente, V., Marchante, V., Dema, H. and Marcilla, A. 2014. Characterization of montmorillonites simultaneously modified with an organic dye and an ammonium salt at different dye/salt ratios: Properties of these modified montmorillonite EVA nanocomposites. *Appl. Clay Sci.* **97-98:** 43-52. DOI: 10.1016/j.clay.2014.06.001

Bundy, W. H. and Ishley, J. N. 1991. Kaolin in paper filling and coating. *Appl. Clay Sci.* **5:** 397-420. DOI: 10.1016/0169-1317 (91) 90015-2

Burst, J. F. 1991. The application of Clay Minerals in Ceramics. *Appl. Clay Sci.* **5:** 421-443. DOI: 10.1016/0169-1317 (91) 90016-3

Corres, M. A., Zubitur, M., Cortazar, M. and Mugica, A. 2013. Thermal decomposition of phenoxy/clay nanocomposites: Effect of organoclay microstructure. *Polym Degrad Stabil.* **98:** 818-828. DOI: 10.1016/j.polymdegradstab.2012.12.004

Dutta, A. 2013. Stabilization of diketo tautomer of curcumin by premicellar cationic surfactants: Spectroscopic, tensiometric, and TD-FT Study. *J Mol Liq.* **187:** 350-388. DOI: 10.1016/j.saa.2012.11.048

El-Shishtawy, R. M. 2009. Dyeing of modified acrylic fibers with curcumin and madder natural dyes. *Fiber Polym.* **10** (5): 617-624. DOI: 10.1007/S12221-010-0617-4

Fischer, H. 2003. Polymer nanocomposites: From Fundamental Research to Specific Applications. *Mater. Sci. Eng.* C **23 :** 763-772. DOI: 10.1016/j.msec.2003.09.148

Gemeay, A.H., El-Shenbiny, A. S., and Zaki, A. B. 2002. Adsorption and kinetic studies of the intercalation of some organic compounds onto Na^+ montmorillonite. *J. Colloid Interface Sci* **245 (1):** 116-125. DOI: 10.1006/jcis.2001.7989

Gil,A., Gandia, L. M., and Vicente, M. A. 2000. Recent Adavances in the Synthesis and Catalytic Applications of Pillared Clays. *Catal. Rev. Sci. Eng* **42:** 145. DOI: 10.1081/CR-10010026

Harris, R.G., Bruce, B. J. and Wells, J. D. 2006. Studies on the adsorption of dyes to kaolinite. *Clay Clay Miner* **54 (4):** 435. DOI: 10.1346/CCMN.2006.0540404

Holzheu, S. and Hoffmann, H. 2002. Adsorption study of cationic dyes having a trimethylammonium anchor group on hectorite using electroptic and spectroscopic methods. *J Colloid Interface Sci.* **245** (1) : 16-23. DOI: 10.1006/jcis.2001.7978

Joseph, L. K., Sanjay, G., Suja, H., Sugunan, S., Nampoori, V. P. N., and Radhakrishnan, P. 2009. Thermal characterization of dye-intercalated K-10 Montmorillonite Ceramics using Photocaustic Technique. *Philos Mag.* **89 10** (1) : 895-905. DOI: 10.1080/14786430902806652

Mousty, C. 2004. Sensors and Biosensors based on Clay-modified Electrodes- New Trends. *Appl. Clay Sci.* **27:** 159-177. DOI: 10.1016/j.clay.2004.06.005

Murray, H. H. 1991. Some Application of Clay Minerals. *Appl. Clay Sci.* **5:** 379-395. doi.org/10.1016/0169-1317 (91) 90014- Z. DOI: 10.1016/0169-1317 (91) 90014-Z

Murray, H. H. 2000. Traditional and new applications for Kaolin, smectite, and palygorskite: A Genreal Overview. *Appl. Clay Sci.* **17:** 207-221. DOI: 10.1016/S0169-1317 (00) 00016-8

Rytwo,G., Nir, S., Crespin, M. and Margulies, L. 2000. Adsorption and interaction of methyl green with Montmorillonite and sepiolite. *J. Colloid Interface Sci* **222:** 12-19. DOI: 10.1006/jcis.1999.6595

Shichi,T., and Takaqi. 2000. Clay Minerals as photochemical reaction fields. J. Photochem. Photobio. *C: Photochem. Rev.* **1 :** 113-130. DOI: 10.1016/S1389-5567 (00) 00008-3

Shinozaki, R. and Nakato, T. 2008. Photochemical behavior of rhodamine 6G dye intercalated in photocatalytically active layered hexaniobate. *Micropor Mesopor Mat.* **113:** 81-86. DOI: 10.1016/j.micromeso2007.11.005

Sinha Ray, S. and Okamato, M. 2003. Polymer/Layered silicate nanocomposites: A Review from Preparation to Processing. *Prog. Polym. Sci.* **28 :** 1539-1641. DOI: 10.1016/j.progpolymsci.2003.08.002

Umbreem, S. 2008. Dyeing Properties of Natural Dyes Extracted from Turmeric and their Comparison with Reactive Dyeing. RJTA **12 (4):** 1-11. doi: 10.1108/RJTA-12-04-2008-B001. DOI: 10.1108/RJTA-12-04-2008-B001

Wang, C.C., Juang, L.C., Hsu, T.C., Lee, C.K., Lee, J.F., and Huang, F.C. 2004. Adsorption of basic dyes onto montmorillonite. *J. Colloid Interface Sci.* **273**(1) **:** 80-86. DOI: 10.1006/jcis.1999.6365

Zeng, Q. H., Yu, A. B., Lu, G. Q. and Paul, D. R. 2005. Clay Based Polymer Nanocomposites: Research and Commercial Development. J. Nanosci. *Nanotechnol.* **5:** 1574-1592. DOI: 10.1166/jnn.2005.411.

(Received June 2017; Accepted October, 2017)

Clay Research, Vol. 36, No. 1, pp. 23-27 (2017)

Preparation and Characterization of ZnO thin Films by Sol-gel Method on Glass Substrates

KHADHER AL-RASHEDI[1], MAZAHAR FAROOQUI[1, 2] AND GULAM RABBANI[1]*

[1]*Post Graduate and research center, MaulanaAzad College, Aurangabad, India 431001*
[2]*Dr. Rafiq Zakaria College for women, Aurangabad*

Abstract–*In this work, nano-crystalline zinc oxide (ZnO) thin film was synthesized using the sol-gel method. The thin film was deposited on a glass substrate at 50°C by using zinc nitrate, methanol, ethanol, polyvinyl alcohol with a magnetic stirrer device and a hot plate. Each deposited thin film annealed in the microwave oven at 200°C. The structure of the prepared thin film was examined by means of X-ray diffraction (XRD). The Shearer formula was used to calculate the size of the film granules. The scanning electron microscopy (SEM) was used to study the surface morphology. UV-VIS measurement was also carried out to study optical properties of a sample by recording transmittance and reflectance data in the range 300 to 700 nm wavelength. All the tests confirmed the existence of a thin layer of ZnO on the glass substrates.*

Key words : Substrates, Sol-Gel Method, Thin Film, zinc oxide, crystallites, dip coating, XRD, SEM, Optical properties, UV.

Introduction

Zinc oxide (ZnO) is an emerging material for a large number of areas (Znaidi *et al.,* 2012).

ZnO is inexpensive (Bayram *et al.,* 2013), and is one of the most common materials for many applications due to its significant physical and chemical properties (Musat *et al.,* 2004). On substrates of glass, using the Sol-gel method, deposition of thin films of ZnO was examined at different rates (Yacine *et al.,* 2015; Poornima *et al.,* 2016; Bousmaha *et al.,* 2016; Klingshirn *et al.,* 2007; Kaneva and Dushkin, 2011; Ibrahim *et al.,* 2013; Kolekar *et al.,* 2011). The thin film is used as gas sensor, in electronic displays, in the fabrication of blue light emitting diodes (LEDs), in surface acoustic wave (SAW) devices, and more (Levinboim *et al.,* 2010; Soosen *et al.,* 2009; Peng *et al.,* 2006), in conductive films, solar cell windows, photoelectric cells, nonlinear optics, bulk and surface acoustic wave devices (Wang, Zhong Lin, 2004; Kulkarn, 2015; Gupta *et al.,* 2010) and cosmetics (Kulkarni, 2015). Unlike many of its competitors, ZnO is inexpensive, relatively abundant, chemically stable, easy to prepare, nontoxic and most of the doping materials that are used with it are also readily available (Yang, T. L., *et al.,* 1998; Tomar, Monika, *et al.,* 2005; Mitsuyu, Tsuneo, *et al.* 1982). Moreover Zinc Oxide is a friend of the environment and easy to synthesize (Wu *et al.,* 2007). ZnO films are deposited by using many methods of deposition. These include various sputtering techniques (Sundaram and Khan, 1997), chemical vapor deposition (CVD) (Li *et al.,* 2002), molecular beam epitaxy (MBE) (Look, David C., *et al.,* 2002), pulsed laser deposition (PLD) (Muth *et al.,* 1999), sol-gel (AL-Rashdi, *et al.,* 2016), filtered vacuum arc (FVA) (Boxman *et al.,* 2003), etc. Only relatively few reports on the properties of ZnO films deposited with FVA are found in the literature (David *et al.,* 2004).

Corresponding Author Email : khadheraskar20@gmail.com

In the present investigation the sol-gel method for synthesis of ZnO Thin Film has been chosen as it is the simplest method, consumes less power and can be carried out in robust atmosphere. The structural properties of the prepared ZnO nanoparticles were studied by using X Ray Diffraction (XRD) and the morphology of ZnO nanoparticles was examined under Scanning Electron Microscope (SEM). The transparency and absorption of synthesized ZnO nanoparticles were studied using a UV visible spectrophotometer.

Experimental

Initially, zinc nitrate solution was prepared by dissolving (2.974g) in pure distilled water (pH ≈ 7.0, Conductivity ≈ 36.00μS/m), then prepared polyvinyl alcohol solution was mixed with zinc nitrate solution in equal volume. The mixed solution was stirred on a hot plate for 3 hours at a room temperature (28°C) under normal atmospheric pressure. After that, the temperature was raised to 50°C with continuous stirring for more than 5 hours. Detailed step by step experimental procedure is illustrated in Fig.1. The glass substrate with dimension (24x40 mm) was dipped in the solution for 60 minutes. Deposited thin film onto glass substrate was dried, and then heated for 10 min in a microwave oven (65 watts, 200°C and at frequency 7 (Hz)).

The thin film was characterized and the morphology of the ZnO thin film was examined using (SEM). The structure and the grain size of the ZnO thin film were studied using X Ray diffraction. The UV-visible spectrum of the sample was obtained by using an SL 210 UV VIS Spectrophotometer-1800, in the wavelength range of 300 to 700 nm.

Results and Discussion

Structural Analysis

The crystal structure and orientation of the ZnO thin films were investigated by X-ray diffractometer. Fig 2 shows XRD patterns of ZnO. The peaks at 2θ = 31.80°, 34.40°, 36.20°, 47.50°, 56.60°, 62.90°, 66.28°, 68°, were assigned to (100), (002), (101), (102), (110), (103), (112), (202), of ZnO, indicating that the samples were polycrystalline wurtzite structure (Zincite, JCPDS 5-0664). No characteristic peaks of any impurities were detected, suggesting that high-quality ZnO were synthesized. The angles that found were identical to angles which were mentioned in reference (Akhtar, Mohd Javed, *et al.*, 2012; Saravanakumar, *et al.,* 2014), in which the number (JCPDS 5- 0664) and (JCPDS 36-1451) was mentioned as a reference for angles with (hkl).

The XRD peak, obtained for the present investigator is identical as reputed Carlier [Alhamed and Wael, 2010] for (100), (002), (101) peak the ZnO film obtained by Sol-gel method from zinc acetate, isopropanol and diethanolamine shows enhanced the intensity of the peak, corresponding to (101), indicating preferential orientation along c-axis and wurtzite structure (Lü, Jianguo, *et al.,* 2010). The poly crystalline nature Na-doped ZnO is also reported wurtzite structure, indicating no effect of Na-doping on the microsfnction of thin film (Ilican *et al.,* 2008).

In few cares, ZnO thin film gives zincite structure with (002) as enhanced intensity [Ilican *et al.,* 2008).

average grain size was 14.7nm. It is calculated by the Scherrer formula: In order to attain the detailed structure information, grain size along z-axis, the

$$D = \frac{0.9\lambda}{\beta \cos\theta} \quad \text{.. (1)}$$

Where λ - wavelength of x-ray (0.154 x 10^{-9}m).

θ - Bragg angle of peaks.

β–Full width at half maximum (FWHM) value.

Morphological Analysis

To obtain insight information about the surface morphology and particle size of the ZnO thin film, SEM was used to get a micrograph of ZnO thin film, which is calcined at 200°C for 10 min as shown in Fig. 3 (A to D).

It shows the surface morphology of ZnO thin films in the form of nano-sheets (Kulkaran, 2015) the SEM image shows a uniform compact surface. The ZnO thin films are crystalline and the average crystallite size of the films is about 14.7 nm, the ZnO thin film obtained by Sol-gel, on porous silicon gines amorphous ZnO thin film (Kim *et al.,* 2011).

Optical Study

The optical properties of the synthesized zinc oxide nanostructures were examined via Spectrum of UV by falling light on the sample, as shown in Figure 4, and measuring the absorption of near and visual light of UV. It is found that the sample absorbs the radiation in the ultraviolet region of 300 nm to 700 nm. The UV-light spectrophotometry analysis showed that the absorption peak at 379.0nm. The energy gap of the thin layer of the zinc oxide was calculated by curve between (h ν) and (α hν)^2. The energy band gap obtained from the extrapolation curve was 3.27eV as shown in Figure 5. Theseresults are compatible with the other works (Ibrahim *et al.,* 2013; Kolekar *et al.,* 2011; Akhtar *et al.,* 2012; Foo *et al.,* 2014).

Conclusion

In this paper, we have developed nanocrystalline ZnO thin films on glass substrate by a Sol-gel strategy. It has been utilized X-ray diffraction study to check the creation of zinc oxide thin films. The XRD spectra demonstrated that the films are of polycrystalline structure. Grain size along z axis was calculated by the Scherrer formula, the grain size of the crystallites was found to be in the average of 14.7nm, the picture of a thin film of zinc SEM was utilized for investigating the morphology of the surface. Oxide obtained was in the form of transparent nano-sheets. The high absorption pinnacle was observed to be at 379 nm, and the band gap energy obtained by extrapolation curve was found to be approximately 3.27eV.

Acknowledgements

I would like to express my thanks to, Dr. Faisal Mohsin muntaser, Ph.D student Ibrahim Mohamed saleh, Ph.D student Manee Hanash and Fahd AL-Ghauri.

References

Akhtar, Mohd Javed, et al. 2012. Zinc oxide nanoparticles selectively induce apoptosis in human cancer cells through reactive oxygen species. *International Journal of Nanomedicine.* 7 : 845.þ

Alhamed, Mounir, and Wael Abdullah. 2010, Structural and optical properties of ZnO: Al films prepared by the sol–gel method. *Journal of Electron Devices.* 7 : 246-252.

AL-Rashdi, Khadher, Farooqui, M. et al. 2016. Metal Oxide Thin Films: A Mini Review. *Journal of Advanced Scientific Research.* 7.1.þ

Aoun, Yacine, et al. 2015. Structural, optical and electrical properties of zinc oxide thin films deposited by a spray pyrolysis technique. *Journal of Semiconductors.* 36.1 : 013002.þ.þ

Bayram, C., et al. "Engineering future light emitting diodes and photovoltaics with inexpensive materials: Integrating ZnO and Si into GaN-based devices. *Proc. of SPIE.* Vol. 8626. 2013.þ.þ

Bousmaha, M., et al. 2016. Realization of p-Type Conductivity in ZnO via Potassium Doping. *Acta Physica Polonica A* 129.6 : 1155-1158.þ

Boxman, R. L., et al. "Society of Vacuum Coaters (SVC) 46th Ann." SVC Techn. Conf. Proc. 2003.

David, T., Goldsmith, S. and Boxman, R.L. 2004. Electro-optical and structural properties of thin ZnO films, prepared by filtered vacuum arc deposition. *Thin Solid Films.* 447 : 61-67.

Foo, Kai Loong, *et al.* 2014. Effect of different solvents on the structural and optical properties of zinc oxide thin films for optoelectronic applications. *Ceramics International.* 40.1 : 753-761.

Gupta, S. K., Aditee Joshi, and Manmeet Kaur. 2010. Development of gas sensors using ZnO nanostructures. *Journal of Chemical Sciences* 122.1 : 57-62.

Ibrahim, N. B., Al-Shomar, S. M. and Ahmad, S. H. 2013. Effect of annealing temperature on the structural and optical properties of nanocrystalline ZnO thin films prepared by sol-gel method. *Sains Malaysiana.* 42(12): 1781-1786.

Ilican, S., Caglar, Y. and Caglar, M. 2008. Preparation and characterization of ZnO thin films deposited by sol-gel spin coating method. *Journal of Optoelectronics and Advanced Materials.* 10.10 : 2578-2583.

Kaneva, N. V. and Dushkin, C.D. 2011. Preparation of nanocrystalline thin films of ZnO by sol-gel dip coating. *Bulg Chem Commun* 43 : 259-263.

Kim, Minsu, et al. "Nanocrystalline ZnO thin films grown on porous silicon by sol-gel method and effects of post-annealing. *Journal of the Korean Physical Society.* 59.2 (2011): 346-352.

Klingshirn, C. 2007. ZnO: From basics towards applications. *Physica Status Solidi.* (b)244.9: 3027-3073.

Kolekar, T. V., Yadav, H. M., Bandgar, S.S. and Deshmukh, P. Y. 2011. Synthesis by sol–gel method and characterization of ZnO nanoparticles. *Indian Streams Research Journal.* 1(1).

Kulkarn, S. S. 2015. Optical and structural properties of zinc oxide nanoparticles. IJARPS, 2: 14-18.

Levinboim, T. 2010. The Raymond and Beverly Sackler Faculty of Exact Sciences The Blavatnik School of Computer Science (Doctoral dissertation, Tel Aviv University).

Li, B. S. *et al.* Growth of high quality ZnO thin films at low temperature on Si. 100. Substrates by plasma enhanced chemical vapor deposition. *Journal of Vacuum Science & Technology A: Vacuum, Surfaces, and Films* 20.1 : 265-269.

Look, David C. *et al.* 2002. Characterization of homoepitaxial p-type ZnO grown by molecular beam epitaxy. *Applied Physics Letters* 81.10 : 1830-1832.

Lü, Jianguo, et al. 2010. Preparation and characterization of Na-doped ZnO thin films by sol–gel method. Physica B: Condensed Matter 405.15 : 3167-3171.

Mitsuyu, Tsuneo, et al. 1982. Piezoelectric thin films of zinc oxide for saw devices. *Ferroelectrics.* 42.1 : 233-240.

Musat, V. *et al.,* 2004. Al-doped ZnO thin films by sol–gel method. *Surface and Coatings Technology.* 180 : 659-662.

Muth, J. F., et al. 1999. Excitonic structure and absorption coefficient measurements of ZnO single crystal epitaxial films deposited by pulsed laser deposition. Journal of Applied Physics 85.11 : 7884-7887.

Nagarani, N. and V. Vasu. 2013. Structural and optical characterization of ZnO thin films by

sol-gel method. *J. Photonics Spintronics.* 2 : 19-21.

Peng, W. Q., Qu, S. C., Cong, G. W., & Wang, Z. G. 2006. Structure and visible luminescence of ZnO nanoparticles. *Materials Science in Semiconductor Processing.* 9 (1) : 156-159.þ

Poornima, K., K. Gopala Krishnan, and S. Dinesh Kumar. 2016. Low Temperature Synthesis and Annealing effect of Transparent ZnO Thin Films on ITO Substrate by Sol-Gel Method. *Indian Journal of Science and Technology* 9.22.

Saravanakumar, M., S. Agilan, and N. Muthukumarasamy. 2014. Effect of Annealing Temperature on Characterization of ZnO thin films by sol-gel method. *International Journal of ChemTech Research.* 6.5 : 2941-2945.

Soosen Samuel, M. Lekshmi Bose and George, K.C. ISSN: 0973-7464 Vol. XVI, (1), (2009), 57-65.

Sundaram, K. B. and A. Khan. 1997. Characterization and optimization of zinc oxide films by rf magnetron sputtering. *Thin Solid Films* 295.1-2 : 87-91.

Tomar, Monika, et al. 2005. Temperature stability of ZnO thin film SAW device on fused quartz. *IEEE Transactions on Device and Materials Reliability.* 5.3 : 494-500.

Wang, Zhong Lin. 2004. Zinc oxide nanostructures: growth, properties and applications. *Journal of Physics: Condensed Matter.* 16.25 : R829.

Wu, Y. L., et al. 2007. Surface modification of ZnO nanocrystals. *Applied Surface Science.* 253.12 : 5473-5479.

Yang, T. L., et al. 1998. Transparent conducting ZnO: Al films deposited on organic substrates deposited by rf magnetron-sputtering. Thin solid films 326.1 : 60-62.

Znaidi, L., et al. 2012. ZnO thin films synthesized by sol-gel process for photonic applications. Acta Physica Polonica-Series A General Physics 121.1 : 165.

(Received October, 2017; Accepted December, 2017)

Clay Research, Vol. 36, No. 1, pp. 28-32 (2017)

Study on the Structural and Optical Properties of Chemically Deposited $Cd_{(1-x)}Zn_xS$ thin Films Using Chemical Bath Deposition Technique

DHANANJAY MUGLE[1*], M.A. BAROTE[2], L. S. RAVANGAVE[3] AND GHANSHYAM JADHAV[1]

[1]*Department of Physics, Shri Chhatrapati Shivaji College, Omerga-413606, Maharashtra, India*
[2]*Department of Physics, Azad College, Ausa-413520, Maharashtra, India*
[3]*Department of Physics, Sant Gadge Maharaj College Loha-431708, Maharashtra, India*

Abstract– *$Cd_{(1-x)}Zn_xS$ (x = 0, 0.2, 0.4, 0.6, 0.8, and 1) thin films were deposited by the chemical bath deposition technique. Thin films were deposited on cleaned glass slide. The structural properties of deposited films were studied by using X-ray diffraction technique. XRD studies revealed that the films were crystalline with cubic and hexagonal structure. Calculated lattice parameter showed good agreement with published data card. It was observed that grain size increased with increase in Zn up to x = 0.4. Further it decreased with increasing Zn. The band gap of the thin films varied from 2.45 to 3.50 eV as x varied from 0.0 to 1.0. It was observed that changes of the small amount of Zn resulted in marked changes in the optical band gap of CdS.*

Key words : *Thin film, $Cd_{(1-x)}Zn_xS$, CBD method, Structural properties, optical properties.*

Introduction

Group II–VI semiconductor thin films have attracted considerable attention because of their broad range of use in the fabrication of solar cells and other optoelectronic devices (Ashokkumar & Muthukumaram, 2014). The conversion of solar energy into a usable form is a probable challenge to the researchers. Group II–VI compounds can form ternary and quaternary alloys with a direct primary band gap task over the entire alloy composition range and with high absorption coefficients power (Jubory 2012). CdZnS ternary thin films have been extensively used as a great bandgap window fabric in hetero junction solar cells and photoconductive devices (Jubory, 2012, Chu *et al.,* 1991)). CdZnS thin films have been prepared by various techniques which include chemical bath deposition, evaporation, spray pyrolysis and metallo organic chemical vapour deposition. Among these techniques, chemical bath deposition (CBD) is the most good-looking because of its useful features over other deposition techniques because it is simple, gives high quality films at low temperatures, requires slow evaporation temperatures and easily coats very large surfaces. (Mosiori *et al.,* 2014). The chemical bath deposition (CBD) technique is at the moment attracting substantial attention to the researcher as it does not need expensive instrumentation like vacuum system and other expensive equipment (Pawar *et al.,* 2011). The starting chemicals are normally available and contemptible. With CBD method, a large number of substrates can be covered in a single run with a good design.

Films prepared by this technique are generally polycrystalline in structure and their properties are influenced by the deposition process (Ashok kumar and Muthukumaram, 2014, Raviprakash *et al.,* 2010).

There are reports (Jubory, 2012) of studying

***Corresponding Author Email :** dhananjayforu@gmail.com.

the effect of Cu doping on the structural and optical properties of $Cd_{0.7}Zn_{0.3}S$. (Hadasa *et al.*, 2014) prepared $Cd_{0.8}Zn_{0.2}S$ compounds doped with different mol % of Cu (1.3, 2.5, 3.8, 5.0 and 6.1) by modified chemical co-precipitation method (CCP method). Bulk $Cd_{0.8}Zn_{0.2}S$ compounds have been prepared by adopting two different ways of mixing the solutions of constituent elements named as CCP-I & CCP-II.(Mosiori *et al.*, 2014) studied the optical and electrical characterization of $Cd_xZn_{x-1}S$ thin films deposited by chemical bath deposition in alkaline conditions. He explained in literature survey that the replacement of CdS with a higher energy gap ternary $Cd_xZn_{1-x}S$ led to a decrease in window absorption loss and lattice mismatching with the Cu in GaSe. He observed that the low processing temperature used in $Cd_xZn_{1-x}S$ as window material could be used to fabricate device at low temperatures. In this present work, cadmium acetate, zinc acetate and thiourea combination have been used as source materials to fabricate thin films of $Cd_{(1-x)}Zn_xS$ with different composition (x = 0.0–1.0) using chemical bath deposition technique.

The growth, structural and optical properties of these films in relation to composition 'x' are reported and discussed, alsodiscussed the relation between energy band gap(eV) and composition parameter(X). and grain size and composition.

Materials and Methods

$Cd_{(1-x)}Zn_xS$ films were deposited on glass substrates with different Zn concentrations (for x = 0, 0.2, 0.4, 0.6, 0.8 and 1) using chemical bath deposition technique. Aqueous solutions used as sources for Cd^{2+}, Zn^{2+} and S^{2-}, were $Cd(CH_3COO)_2$ $2H_2O$, $Zn(CH_3COO)_2$ and $2H_2O$ and $CS(NH_2)_2$ respectively. The entire chemicals used in the present study and reagent used were of analytical reagent grade. In one of the film preparation of ZnS(x=1) mixed (10ml) $ZnSO_4$ + (4ml)TEA(tri either ammain) in a glass beaker and stirred well for 2min and then added (10ml) Thaourea+(10ml) NH_3 + (4ml)NaOH in a beaker and added deionized water to fill the beaker up to 150ml. Glass slides were washed with detergent and rinsed in acetone before the deposition of the films. The cleaned substrate was kept dipped in deionized water before use. The well-cleaned glass substrates were slowly introduced into the bath vertically after obtaining the homogeneous solution. The desired pH value, 9 to 11 was achieved by the addition of aqueous ammonia solution proportionally into the mixture in the chemical bath. The temperature of the mixed solution was maintained at 75^{0}C using a constant temperature under continuous stirring. The films were prepared under continuous stirring for 1 h. The deposited films were cleaned several times with de-ionized water. After that film were dried in sun and air.

Result and Discussions

Structural analysis

XRD study revealed that the film was crystalline with cubic and hexagonal structure. It was observed that grain size increased with increasing Zn in composition x upto(x = 0.0 to 0.4) further it decreased with decreasing Cd upto (x=0.6 to 1) as shown in the fig.1 and its corresponding peak value.

(Barote *et al,* 2010) showed that X-ray diffractograms of 'as-grown' samples exhibited polycrystalline nature of cubic phases for CdS and PbS tgether and hexagonal phase for CdS

Table 1. *Show energy band gap with composition x.*

X	eg
0.0	2.45
0.2	2.60
0.4	2.75
0.6	2.95
0.8	3.22
1.0	3.50

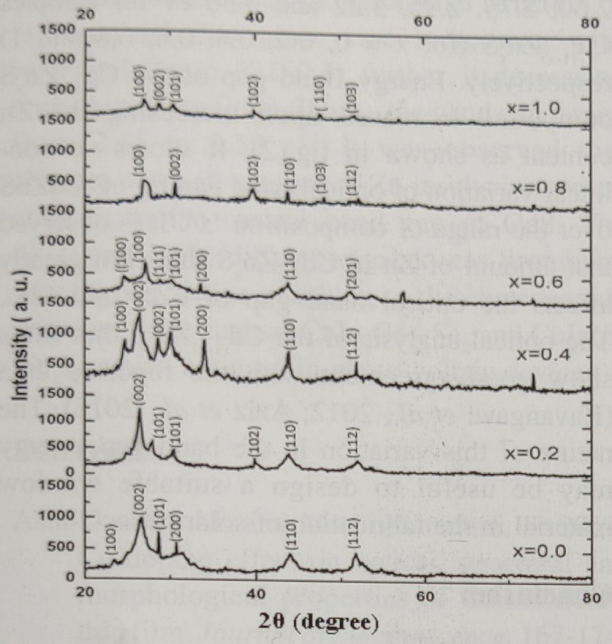

Fig. 1. *XRD Spectra of Cd(l-x)ZnxSsynthesized for (X=0.0, 0.2, 0.4, 0.6, 0.8 and 1.0)*

alone. (Dutkova *et al.,* 2008) also reported a phase transition from hexagonal to cubic with an increase of Zn content of $Cd_{1-x}Zn_xS$ nanoparticles. (Jubory 2012)also showed that the grown $Cd_{0.7}Zn_{0.3}S$ thin films were polycrystalline with a hexagonal structure (Singh *et al.,* 2014) observed that the XRD pattern showed nano crystalline phase with cubic and hexagonal structure. The doped film showed broadening of peaks in XRD pattern

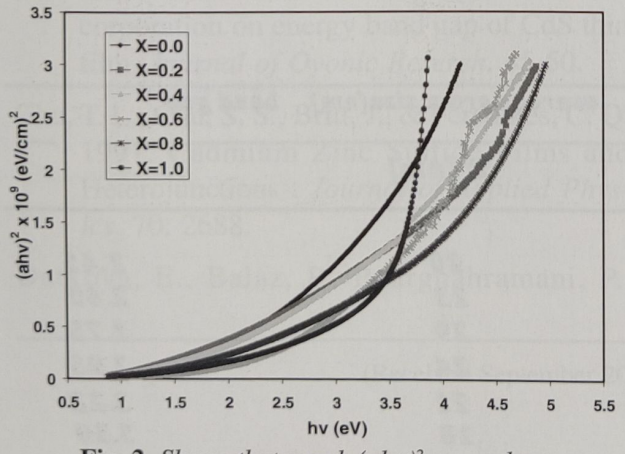

Fig. 2. *Shows that graph (ahν)² versus hν.*

The XRD pattern of the $Cd_{(1-x)}Zn_xS$ as shown in fig.1 indicates presence of prominent peak (100), (002), (101), (200), (110) and (112) plane of x=0.0 (CdS) which showed cubic and hexagonal structure. The intensity of (002) peak increased with increasing Zn upto (x=0.0 to 0.4) and peak (100), (002), (110), (102), (110) and (103) plane of x=1.0 (ZnS) material showed hexagonal structure. The intensity of (100) peak decreased with decreasing cd upto (x=0.6 to 1). The standard crystallographic data for CdS and ZnS were taken from JCPDS card no. 80-0006 and 36-1450 respectively which showed good agreement.with observed data

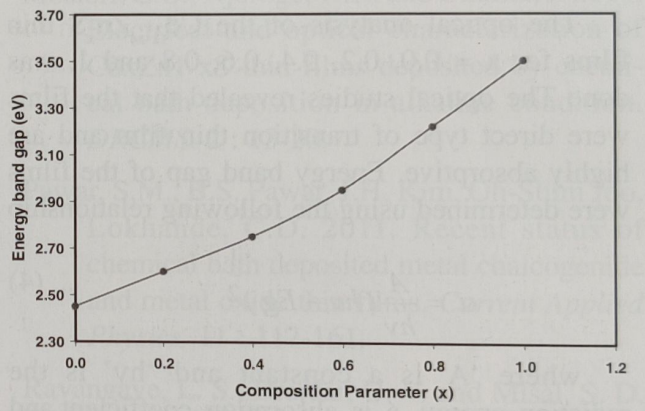

Fig. 3. *Shows the graphical representation of energy band gap eV with composition(x)*

Table 2 shows the lattice parameters a and c for hexagonal and cubic systems calculated using equation 1 and 2 (Raviprakash *et al.,* 2010), (Ravangave *et al.,* 2012), (Aziz *et al.,* 2016). Lattice parameters of CdS for (X=0.0, 0.2, 0.4) and ZnS for (X=0.6, 0.8, 1.0) have been calculated

$$\frac{1}{d^2} = \frac{4}{3}\left(\frac{h^2 + hk + k^2}{a^2}\right) + \frac{l^2}{c^2} \quad \text{.. (1)}$$

$$\frac{1}{d^2} = \frac{4}{3}\left(\frac{h^2 + hk + k^2}{a^2}\right) \quad \text{.. (2)}$$

Where d is interplanar distance, a and c are lattice constants, and h, k, and l are the miller indices of the plane.

The grain size 'D' of the samples was obtained by using 'Scherrer's formula (Barote *et al.*, 2010)

$$D = \frac{0.94\lambda}{\beta \cos\theta} \quad .. (3)$$

Where λ is the wave length of X-ray used (1.54 nm C_uK_α line), b is the broadening of the diffraction peak measured at half of its maximum intensity (FWHM) and ε is the Braggs angle. The calculated grain size and lattice constant is as shown in Table 2.

Optical analysis

The optical analysis of the $Cd_{(1-x)}Zn_xS$ thin films for x = 0.0, 0.2, 0.4, 0.6, 0.8 and 1. was done The optical studies revealed that the films were direct type of transition thin film and are highly absorptive. Energy band gap of the films were determined using the following relationship

$$\alpha = \frac{A}{h\nu}(h\nu - Eg)^{\frac{1}{2}} \quad .. (4)$$

where 'A' is a constant and 'hν' is the radiation energy, á is absorption coefficient,and Eg is energy band gap. The experimentally observed values of $(\alpha\ h\nu)^2$ were plotted against hν is shown in Fig.(2) for a different composition and Eg values were calculated from graph

Estimated values of the energy gap were 2.45, 2.60, 2.75, 2.95, 3.22 and 3.50 ev for samples $Cd_{(1-x)}Zn_xS$ (for x = 0, 0.2, 0.4, 0.6, 0.8 and 1) respectively. Energy Band gap of the $Cd_{1-x}Zn_xS$ compound increased upon increasing the Zn content as shown in fig.(2). It shows e non-linear variation of optical band gap Eg of CdZnS over the range of composition 'x'. It is observed that amount of Zn in $Cd_{1-x}Zn_xS$ thin film greatly affects the optical band gap of CdS thin film. The optical analysis of the $Cd_{(1-x)}Zn_xS$ thin films show good agreement with the reported data (Ravangave *et al.*, 2012; Aziz *et al.*, 2016). The nature of this variation in the band gap, energy may be useful to design a suitable window material in the fabrication of solar cells.

Conclusion

XRD studies showed that the films are

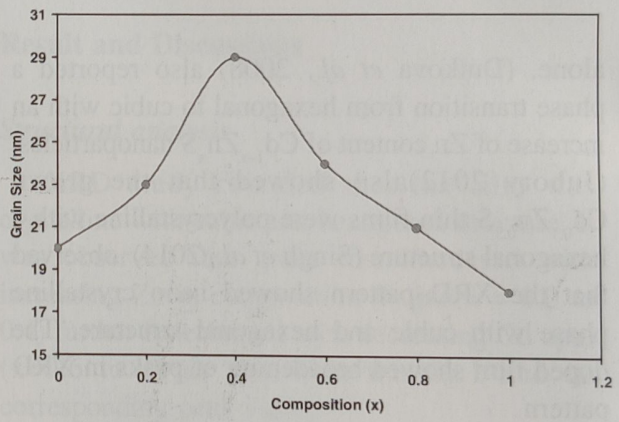

Fig. 4. *Shows graph of grain size and composition (x)*

Table 2. *Structural parameters of $Cd_{1-x}Zn_xS$ thin films.*

Composition 'x'	Material	lattice constant (A°)		average grain size(nm)	band gap
	$Cd_{1-x}Zn_xS$	a	c	D (nm)	
X= 0.0	CdS	4.17	6.80	20	2.45
X= 0.2	$Cd_{0.8}Zn_{0.2}S$	3.99	6.80	23	2.60
X= 0.4	$Cd_{0.6}Zn_{0.4}S$	4.11	6.71	29	2.75
X= 0.6	$Cd_{0.4}Zn_{0.6}S$	4.10	6.65	24	2.95
X= 0.8	$Cd_{0.2}Zn_{0.8}S$	3.80	6.20	21	3.22
X= 1	ZnS	3.80	6.20	18	3.50

crystalline with cubic and hexagonal structure. It is observed that grain size increasing with increased Zn in (0.0-0.4) further it decreasing with decreasing Cd in (0.6-1). the band gap varied from 2.45 to 3.50 eV. It was observed that changes of small amount of Zn results in marked changes in the optical band gap of CdS. The (002) and (100) diffraction peak was prominent which gives lattice matching to the chalcogenide semiconductor such as $CuIn_xGa_{1-x}Se_2$ and $CuIn(S_{1-x}Se_x)_2$, which are used in photo-voltaic devices

References

Ashokkumar, M. and Muthukumaram, S. 2014. Cu doping effect on optical, structural and morphological properties of Cd0.9Zn0.1S thin film. *Journal of Luminescence.* 167-174.

Aziz, S., Rezagholipour, H., Dizaji, and Ehasani, M.H. 2016. Structural and optical properties of Cd1-xZnxS (x=0, 0.4, 0.8, 1) thin film prepered using the precursor obtained from microwave irradiation process. *Optik.* 127: 7104-7114.

Barote, M. A., Yadav, A. A., Deshmukh, L. P. and Masumdar, E. U. 2010. Synthesis and characterization of chemically deposited Cd1-xPbxS thin film. *Journal of Non-Oxide Glasses.* 2 : 151-165.

Barote, M. A., Yadav, A. A., Suryawanshi, V. R., and Masumdar, E. U. 2011. Effect of Pb Incorporation on energy band gap of CdS thin film. *Journal of Ovonic Reserch.* 45-50.

Chu, T. L., Chu, S. S., Britt, J., & Feredikes, C. Q. 1991. Cadmium Zinc Sulfide Films and Heterojunctions . *Journal of Applied Physics.* 70: 2688.

Dutkova, E., Balaz, P., Pourghahramani, P., Nguyen, A. V., Sepelak, V., Feldhoff, A., et al. 2008. *Solid State Ionics.* 179 : 1242.

Hadasa, K., Yellaiah, G. and Nagabhushanam, M. 2014. Optical transport properties of Cd0.8Zn0.2S:Cu compound prepeared by modified co-presipitation method. *Optik.* 125 : 6602-6608.

Jubory, A. A. 2012. Study on the effect of copper doping on the structural and optical properties of Cd0.7Zn0.3S Nanocrystalline thin films prepeared by chemical bath deposition. *International Journal of Scince and Technology.* 2 : 707-712.

Mosiori, C.O., Njoroge, W.N. and Okumu, J. 2014. Electrical and optical characterization of CdxZn1-xS thin films deposited by chemical bath deposition in alkaline condition. *DRCMS.* 2 : 13-20.

Pawar, S,M., B.S. Pawar, J.H. Kim, Oh-Shim Joo, Lokhande, C.D. 2011. Recent status of chemical bath deposited metal chalcogenide and metal oxide thin films. *Current Applied Physics.* 11 : 117-161.

Ravangave, L. S., Brajdar, U. V. and Misal, S. D. 2012. The effect of ionic composition on structural and optical properties of CdxZn1-xS thin film growth by spry pyrolesys method. *International Jouranal of Scintific Reserch Journal.* 10 : 193-198.

Raviprakash, Y., Kasturi, V., Bangara, V. and Shivkumar, G. K. 2010. Growth structural and optical properties of CdxZn1-xS thin film grown by spry pyrolysis technique. *Current Applied Physics.* 10 : 193-198.

Singh, S. and Shrivastava, A. K. 2014. Synthesis growth and characterization of rare earth doped (CdZnS) thin film. *IJIRSET.* 3 (6).

(Received September 2017; Accepted December 2017)

Clay Research, Vol. 36, No. 1, pp. 33-45 (2017)

Role of Calcium Carbonate and Palygorskite in Enriching Exchangeable Magnesium to Impair Drainage of Vertisols of Semi-Arid Western India

SWATI P. ZADE[1], P. CHANDRAN[2] AND D. K. PAL[3]

[1]Assistant Professor, College of Agriculture, Vasantrao Naik Marathwada Krishi Vidyapeeth, Parbhani
[2]Present and [3]Former Principal Scientist, Indian Council of Agricultural Research-National Bureau of Soil Survey and Land Use Planning, Nagpur

Abstract–*Shrink-swell soils (Vertisols and their intergrades) as one of the major soils support high crop production in Maharashtra, Madhya Pradesh, Andhra Pradesh and northern Karnataka. Vertisols occur extensively in the states of Maharashtra, occupying 36% of the total area. Under rain-fed conditions, the yield of deep-rooted crops on Vertisols depends primarily on the amount of rainwater stored at depth in the soil profile and the extent to which this soil water is released during crop growth. Both the retention and release of soil water are governed by the nature and content of clay minerals, and also by the nature of the exchangeable cations such as sodium and magnesium. The hydraulic conductivity and clay dispersion of swell shrink soils as a function of exchangeable sodium and magnesium are two important soil properties that need to be understood in view of their concurrent pedogenic processes like clay illuviation, calcium carbonate formation and enrichment of exchangeable sodium and magnesium in the subsoils. Therefore, the present study was undertaken with thirteenVertisols of semi-arid tropical (SAT) western Maharashtra. Results of this study indicate the formation of pedogenic calcium carbonate (PC) triggers the chemical reaction for the concomitant enrichment of exchangeable sodium(ESP) and exchangeable magnesium percentage (EMP) in the subsoils and development of Sodic Haplusterts (ESP > 5) witha low value of sHC (<10 mmhr^{-1}). It was interesting to note similar low values of sHC in Typic Haplusterts endowed with palygorskite mineral. Results indicate that when the impairment of sHC in Sodic Haplusterts is primarily due to increase in ESP and EMP, the enrichment of EMP caused by the presence of palygorskite in Typic Haplusterts is equally capable of impairing the drainage (in terms of hydraulic properties) of Vertisols. This is the opposite effect from that of saturation with Ca^{2+} ions, which leads to blocking of small pores in the soil. This suggests that Mg^{2+} ions are less efficient than Ca^{2+} ions in flocculating soil colloids and also in creating strong plasma separation although the United States Salinity Research Laboratory grouped Ca^{2+} and Mg^{2+} together as both the ions improve soil structure. This fact assumes a great importance in the use and management of palygorskite endowed Vertisols especially when they are still classed as Typic Haplusterts, suggesting no sign of natural soil degradation in them.*

Key words : SAT Vertisols, Maharashtra, Exchangeable sodium percentage, Exchangeable magnesium percentage, Saturated hydraulic conductivity, Natural soil degradation, Palygorskite

Vertisols and their intergrades as one of the major soils support agriculture in India. These are important soils in terms of high crop production in Maharashtra, Madhya Pradesh, Andhra Pradesh and northern Karnataka. Vertisols occur extensively in the state of Maharashtra, occupying 36% of the total area (Bhattacharyya *et al.*, 2013). Majority of these soils occurs in the lower piedmont plains or valleys and in micro-depressions, and are developed in the alluvium of weathered Deccan basalt (Pal and Deshpande 1987). These soils are used for many purposes, including the production of cotton, soybean and sorghum. Vertisols are often difficult

***Corresponding Author Email :** spzade@yahoo.co.in

to cultivate, particularly for small farmers using handheld or animal drawn implements. Subsoil porosity and aeration are generally poor and roots of annual crops do not penetrate deeply. The drainage or hydraulic conductivity of smectitic soils is strongly dependent on the type of exchangeable cation in soils and the salt concentration of percolating solution. Saturated hydraulic conductivity (sHC) tends to decrease with increasing exchangeable sodium percentage and decreasing salt concentration. Adsorbed Ca^{2+} stabilizes the soil structure and counteracts the dispersive effect of Na^{+}. U.S. Salinity Laboratory Staff (Richards, 1954) reported that Ca^{2+} and Mg^{2+} were similarly beneficial in developing and maintaining soil structure. Alperovitch *et al.* (1981) suggested that in calcareous montmorillonitic soils, exchangeable Mg had no direct effect on the HC and clay dispersion in presence of Ca. Conversely in non-calcareous, highly weathered soils, if the Na-Mg soils are leached with distilled water, exchangeable Mg appeared to affect both HC losses and clay dispersion. Earlier studies on chemical degradation of Vertisols (Kadu *et al.*, 1993; Balpande *et al.*, 1996; Pal *et al.*, 2006) indicated that in soils even with ESP <5, the sHC showed a decline with pedon depth. However, despite an increase in exchangeable magnesium percentage (EMP) with depth in general, no significant correlation was obtained between sHC and EMP, possibly because of limited data. The gradual enrichment of EMP with depth, however, did not always reflect in a sharp increase of water dispersible clay (WDC) in calcareous and non-sodic Typic and Aridic Haplusterts (ESP <<5) (Balpande *et al.,* 1996; Pal *et al.*, 2006). But a sharp increase in both EMP and WDC in calcareous and sodic (ESP> 5 < 15) Vertisols (Sodic and Calcic Haplusterts) was observed (Pal *et al.*, 2006). It was thus safely assumed that the decline in drainage in terms of hydraulic properties of Vertisolsis also get affected by the presence of Mg on soil's exchange sites, suggesting that saturation of Vertisols not only with Na^{+} ions but also with Mg^{2+} ions leads to dispersion of clay in a certain extent. The dispersed clay particles block the micro- and macro-pores of soil systems causing reduced HC in the subsoil.Considerable research effort has been expended on an attempt to understand the role of adsorbed Na ion on soil physical properties but the effect of Mg ions is less known particularly in soils high activity clays. It is now well understood that the formation of pedogenic calcium carbonate (PC) and clay illuviation are the two concurrent contemporary pedogenic processes in SAT Vertisols of the Holocene period (Pal *et al.*, 2009, 2012). Due to these pedogenic processes, the precipitation of $CaCO_3$ as PC enhances the pH and also the relative abundance of not only Na^{+} but also Mg^{2+} ions in soil exchange and in solution (Pal *et al.,* 2012). Enrichment of EMP is also caused by the reported presence of Mg-rich palygorskite mineral in Vertisols of Maharashtra (Zade, 2007; Hillier and Pharande, 2008; Kolhe, 2011). Under rain-fed conditions, the yield of deep-rooted crops on Vertisols enriched either with EMP or ESP and EMP together would depend primarily on the amount of rain water stored at depth in the soil profile and the extent to which this soil water is released between the rains during crop growth. In view of this predicament, there is an urgent need to understand the mechanism on the enrichment of EMP and ESP amidst the formation of PC and the release of Mg ions from palygorskite. The present study, with 13 Vertisols (including Typic and Sodic Vertisols with and without palygorskite mineral) of Marathwada region, Maharashtra (Table 1) was undertaken to pinpoint the respective role of PC and palygorskite in developing EMP enriched subsoils and its influence in declining the drainage of semi-arid tropical (SAT) Vertisols.

Materials and Methods

Thirteen SAT Vertisols were selected in the districts of Buldhana, Parbhani, Latur,

Osmanabad, Beed, Jalna and Aurangabad of Maharashtra state (Table 1). These Vertisols are developed in the alluvium of the Deccan basalt. Pedons 1,2,4,7,8,9,12 and 13 were keyed out as Typic at the subgroup level, where as pedons 3,5,6,10 and 11 qualified for Sodic. All Vertisols excepting the pedons 5 and 7 contain Ca-zeolites as confirmed by the XRD method (Jackson, 1979) and micro-morphological soil thin section studies (Zade, 2007).

The characteristics of each pedon and its individual horizons were described following the procedure of the Soil Survey Manual (Soil Survey Division Staff, 1993). Both sphenoids and slickensides observed in the field confirm the presence of slickensided B horizons (Bss)(Soil Survey Staff, 1999). Particle size distribution was determined by the international pipette method after the removal of organic matter, $CaCO_3$and free Fe oxides.Sand (2000-50 μm), silt (50-2 μm) and clay fractions (<2 μm and <0.2 μm)were separated using the size segregation procedure of Jackson (1979).

The $CaCO_3$,pH, exchangeable Na and K were determined on total fine earth (<2mm) by standard methods (Richards, 1954). Exchangeable calcium and magnesium were determined from <2 mm sieved samples by leaching with 1N NaCl solution (Piper, 1950) and titrating the leachate against saturated EDTA solution as per the method of Richards (1954). The saturated hydraulic conductivity (sHC) was determined by constant head method as described by Richards (1954). The water dispersible clay (WDC) was determined by taking 10g of soil and then shaking on an end to end shaker for 8 hours. Suspension aliquots were drawn by following the international pipette method (Richards, 1954; Balpande, 1993). For identification of clay minerals, the silt and clay fractions were subjected to X-ray examinations of the parallel oriented samples saturated with Ca and K, using a Philips diffractometer with Ni filtered CuKα radiation at a scanning speed of $2^{o}2\theta$/min. Glycolation and different thermal pretreatments as required were given to distinguish and confirm the type of mineral present (Jackson, 1979). For identification of palygorskite mineral by XRD method, water dispersible clays and silts were used because clays prepared by removing the cementing agents of soils (organic matter, $CaCO_3$ and free Fe_2O_3) did not show the presence of this mineral as this mineral often gets destroyed by such pretreatments (Sombroek, 1981). Limited XRD data on the presence of palygorskite in Vertisols do not however yield sharp peak of palygorskite of 1.05 nm. Instead, a broad and moderate peak around 1.05 nm is generally observed (Pal *et al.,* 2003a; Kolhe *et al.*, 2011). In the present study, after a careful examinationa very small and broad peak around 1.05nm was observed in absence of mica (Figs 2 and 3) and the same was considered to be due to the presence of palygorskite, which was supported by exchangeable Mg enrichment down the pedon depth in poorly drained Typic Haplusterts (pedon 9, Table 2). Undisturbed soil blocks (8cm long, 6cm wide and 5cm thick) were collected from soil horizons, and thin sections were prepared by the methods of Jongerius and Heintzberger (1975). They were described according to the nomenclature of Bullock *et al.* (1985).

Results

Morphological Properties

The studied Vertisols are deep to very deep (100 to more than 150 cm). The cracks were 2 to 10 cm wide at the surface and extended upto a depth of 20 to 60 cm. The pressure faces were observed in all the profiles. Slickensides were tilted to an angle of 45-60 degree from horizontal. The peds broke into small subangular blocky to angular blocky peds. The soils were very dark gray to dark yellowish brown (10YR 3/1.5 to 10YR 4/4). The surface horizon of all the soils generally had subangular blocky structure and slightly hard to hard (dry) and friable to

Table 1. *General properties of the Vertisols selected from different districts and their mean annual rainfall (MAR) and temperature (MAT)*

Pedon No.	Soil Series (Soil Taxonomy) (District)	Parent Material	Latitude	Longitude	MAR[1] (mm)	MAT[1] (°C)	Topography	Special features
1	Chandaj (Very fine, smectitic, isohyperthermic, Typic Haplusterts) (Parbhani)	Basaltic alluvium with zeolites	19°32'42" N	76°42'20" E	957	26.9	Plateau	3-5 cm cracks up to 10-15cm.
2	Satgaon (Very fine, smectitic, isohyperthermic, Typic Haplusterts) (Buldhana)	Basaltic alluvium with zeolites	20°23'53" N	76°13'45" E	899	25.7	Valley	No cracks observed at the time of sampling
3	Kalegaon (Fine, smectitic, isohyperthermic, Sodic Haplusterts) (Jalna)[2]	Basaltic alluvium with zeolites	19°49'15" N	75°59'57" E	840	27.2	Subdued plateau	3-5 cm cracks up to 10-15cm
4	Adgaon (Very fine, smectitic, isohyperthermic, Typic Haplusterts) (Jalna)	Basaltic alluvium with zeolites	20°27'32" N	75°49'20" E	840	27.2	Undulating landscape valley	1-2 cm cracks up to 40 cm and beyond
5	Khasgaon (Very fine, smectitic, isohyperthermic, Sodic Haplusterts) (Osmanabad)[2]	Basaltic alluvium	18°14'59" N	75°29'31" E	809	25.8	Subdued plateau	No cracks observed at the time of sampling
6	NaliWadgaon (Fine, smectitic, isohyperthermic, Sodic Haplusterts) (Osmanabad)[2]	Basaltic alluvium with zeolites	18°35'58" N	75°30'29" E	809	25.8	Watershed basin of interhill	3-4 cm cracks up to 40cm
7	Gategaon (Very fine, smectitic, isohyperthermic, Typic Haplusterts) (Latur)	Basaltic alluvium	18°24'26" N	76°24'37" E	802	26.7	Subdued plateau and beyond	3-5 cm cracks on surface up to 60 cm
8	Sawargaon Deoni (Very fine, smectitic, isohyperthermic, Typic Haplusterts) (Latur)	Basaltic alluvium with zeolites	18°17'20" N	77°06'43" E	802	26.7	Subdued plateau	2-3 cm cracks extend up to 30-40cm
9	Kajal Hipperga (Very fine, smectitic, isohyperthermic, Typic Haplusterts) (Latur)	Basaltic alluvium with zeolites	18°40'14" N	76°53'10" E	802	26.7	Subdued plateau	3-5 cm cracks up to 30-45
10	Bhalgaon (Fine, smectitic, isohyperthermic, Sodic Haplusterts) (Aurangabad)[2]	Basaltic alluvium with zeolites	19°49'38" N	75°28'42" E	792	26.05	Subdued plateau	3-4cm cracks up to 40-45cm in the adjoining field.
11	Babhulgaon (Fine, smectitic, isohyperthermic, Sodic Haplusterts) (Aurangabad)[2]	Basaltic alluvium with zeolites	20°02'40" N	74°58'03" E	792	26.05	Undulating land interhill valley	4-5cm up to 50-60 cm and beyond.
12	Patrud (Fine, smectitic, isohyperthermic, Typic Haplusterts) (Beed)	Basaltic alluvium with zeolites	19°04'15" N	76°12'10" E	685	26.15	Subdued plateau	3-5 cm cracks up to 40 cm
13	Raurgaon (Very fine, smectitic, isohyperthermic, Typic Haplusterts) (Beed)	Basaltic alluvium with zeolites	18°45'43" N	75°42'20" E	685	26.15	Subdued plateau	3-5 cm cracks up to 45 -50cm.

[1]www.indiastat.com; [2]As per criteria of sodic shrink-swell soils advocated by Balpande *et al.* (1996)

moderately friable (moist) consistency (Zade, 2007)). Calcium carbonate was observed throughout the depth of all soils. In pedons 1, 5, 7, 8, 9, the effervescence (with 10% HCl) was slight whereas in pedons 2, 3, 4, 6, 10, 11, 12 and 13, it was strong to violent, which is attributed to the presence of diffuse powdery form of $CaCO_3$.

Physical and Chemical Properties

The soils contain 30-80 per cent clay and 18 to 60 per cent of this is the fine clay (<0.2 μm). Based on mean weighted average, pedons 1, 2, 4, 5, 7, 8, 9, and 13 are classed of clay as very fine and the remaining pedons as fine (Soil Survey Staff, 2014). The clay content gradually increased with depth and in some pedons decreased in the Bss3 and C horizons. The fine

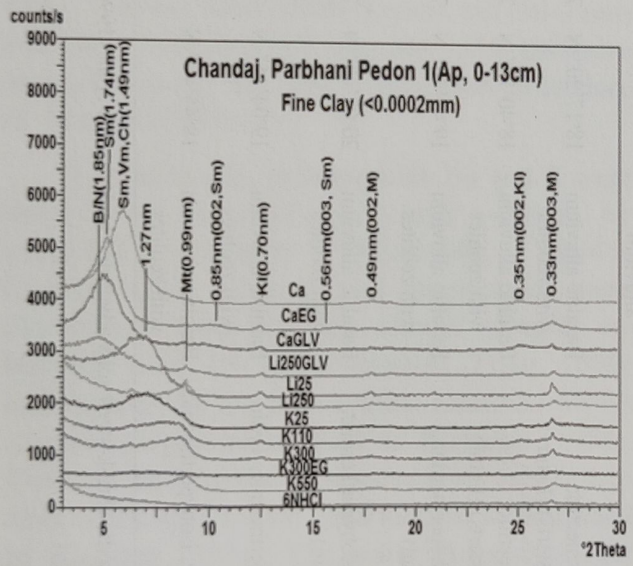

Fig. 1. *Representative XRD patterns of the fine clay fractions of Chandaj, Parbhani. Ca = Ca-saturated, CaEG = Ca-saturated plus glycol vapour, CaGLV = Ca-saturated plus glycerol vapour, Li250GLV=Li-saturated and heated to 250°C(16hrs.) plus glycerol vapour , Li25 = Li-saturated at 25°C, Li250 = Li-saturated and heated to 250°C, K25/110/300/550°C = K-saturated and heated to 25°C, 110°C, 300°C and 550°C, K300EG= K-saturated plus ethylene glycolvapour and heated at 300°C, 6NHCl = HCl treated clay, B/N = beidellite/nontronite, Sm= smectite, Vm=vermiculite, Ch=Chlorite, Mt = Montmorillonite, Kl=kaolin.*

clay fractions (<0.2 μm) of all soils contain dominant proportions (>80%) of fairly well crystallized smectite with very minor amounts of kaolin. The expansion of smectite beyond 1.4 nm with glycolation of the K-saturated and heated (300°C) sample, indicated that the smectite possesses low charge (Fig 1). Fine clay smectite in these soils is a low charge di-octahedral smectite and is nearer to montmorillonite in the montmorillonite-nontronite series (Zade, 2007).

The sHC of soils varied from 0.01 to 5.5 cm hr^{-1}. In Typic Haplusterts (Pedons 1, 2, 4, 7, 8, 9, 12 and 13), the sHC varied from 0.7 to 5.5 cm hr^{-1} and the decrease with depth is gradual but in Sodic Haplusterts (Pedons 3, 6, 10 and 11)it decreased rapidly with depth with a least value of <1 cm hr^{-1} (Table 2). The water dispersible clay (WDC) varied from 4.2 to 40.4 per cent and in non-sodic soils (Typic Haplusterts) it showed a gradual increase whereas in sodic soils (Sodic Haplusterts), it rapidly increased with depth (Table 2). A significant positive correlation was observed between the WDC and the ESP (r= 0.397 at 1% level, Table 3). The non-sodic soils are neutral to mildly alkaline and sodic soils are highly alkaline in reaction and the pH increases with depth in both the non-sodic and sodic soils.

Calcium was the dominant exchangeable cation followed by Mg^{2+}, Na^{+} and K^{+} except some Sodic Haplusterts (Pedons 6, 10 11and 13) where Mg^{2+} is the dominant cation. In general exchangeable calcium decreases and exchangeable Na^{+} and Mg^{2+} increases with depth. The ESP varied from <1 to 37. The ESP value of the surface soil is <5, whereas in subsurface it was >5 in Sodic Haplusterts (Pedons 3, 5, 6, 10 and 11). In Typic Haplusterts (Pedons 1, 2, 4, 7, 8, 9, 12 and 13), the ESP value is less than 5 in both surface and subsurface horizons. It was observed that the decrease in Ca/Mg ratio and Ca/(Mg+Na) ratio (Table 2) appears to be related to development of subsoil sodicity in Sodic Haplusterts (Pedons, 3, 5, 6, 10 and 11).

Table 2. *Sodicity related physical and chemical properties of soils*

Depth (cm)	Exch. Ca/Mg	ECP[1]	EMP[2]	ESP[3]	WDC	Exch. Ca/(Mg+Na)	sHC cm/ hr[5]	% $CaCO_3$/ (HCO_3/Ca)
Pedon 1 : Chandaj (Parbhani) - Very fine, smectitic, isohyperthermic, Typic Haplusterts								
0-13	4.8	79.7	16.6	0.8	17.6	4.6	3.0	6.7/(0.5)
13-28	5.8	83.1	14.4	0.5	20.7	5.6	4.9	6.3/(1.5)
28-45	5.2	81.9	15.8	0.5	26.9	5	5.6	6.5/(1.5)
45-75	4.5	80.2	17.9	0.4	28.2	4.4	4.2	6.8 /(0.7)
75-108	3.7	76.8	20.8	0.6	21.4	3.6	4.2	6.7/(0.7)
Pedon 2 : Satgaon (Buldhana) - Very fine, smectitic, isohyperthermic, Typic Haplusterts								
0-6	3.1	73.3	23.3	1.3	22.9	3	1.5	6.0/(0.7)
19-Jun	2.9	72.6	25	1.2	20.1	2.8	2.4	7.8/ (0.6)
19-35	2.9	72.9	25.1	1.6	21.1	2.7	4.0	9.5/ (1.1)
35-51	2.2	67.3	30.6	1.7	22.3	2.1	5.0	14.8/(0.6)
51-118	1.5	57.7	39.3	1.6	18.4	1.4	3.4	16.7/(0.7)
118-130+	1.3	53	42	3.7	20.9	1.2	0.9	24.9/ (1.1)
Pedon 3 : Kalegaon (Jalna) - Fine, smectitic, isohyperthermic, Sodic Haplusterts								
0-14	2	64.6	31.9	1.4	18.5	1.9	1.0	15.0/(0.3)
14-36	1.6	57.1	36.5	4.8	19.4	1.4	1.2	14.2/(0.4)
36-57	1.3	51.5	39.2	7.9	20.2	1.1	0.4	14.4/(0.9)
57-87	0.8	37.1	47.9	12.5	29.5	0.6	0.03	15.5/(0.9)
87-114	0.7	33.6	47.1	17.9	27.3	0.5	0.03	17.0/(1.1)
114-130+	0.8	37.9	44.1	17.7	20.3	0.6	0.1	24.4/(0.4)
Pedon 4 : Adgaon (Jalna) - Very fine, smectitic, isohyperthermic, Typic Haplusterts								
0-12	2.9	70.8	24.4	1	17.4	2.8	1.7	13.2/(0.6)
Dec-33	1.9	63.4	33.4	1.1	16.5	1.8	3.2	11.7/(0.6)
33-49	1.4	56.5	40.4	1.6	12.3	1.3	3.3	14.6/(0.6)
49-82	0.9	46.3	51	1.9	11.4	0.9	4.1	20.5/(0.6)
82-105	1.1	50.4	45.9	2.5	10.1	1	2.4	21.0/(1.5)
105-129+	1.1	51.2	45.3	2.4	12.5	1.1	2.5	24.5/(1.5)
Pedon 5 : Khasgaon (Osmanabad)- Very fine, smectitic, isohyperthermic, Sodic Haplusterts								
0-14	2	63.9	31.9	3.2	11.3	1.8	0.8	8.6/(1.2)
14-30	1.8	60.7	33.5	4.5	13.4	1.6	1.0	9.8/(1.2)
30-53	2.6	67.7	25.6	6.1	14.5	2.1	1.2	10.1/(0.7)
53-77	2.9	68.5	27.4	7.2	16.0	2.2	1.6	9.9/(0.6)
77-102	2.3	63.9	27.6	7.6	15.0	1.8	1.9	11.4(/0.1)
102-150	1.5	55.9	36.5	5.9	8.5	1.3	0.9	15.5/(0.9)
Pedon 6 : NaliWadgaon (Osmanabad) - Fine, smectitic, isohyperthermic, Sodic Haplusterts								
0-13	1.4	55.7	39.9	3	9.0	1.3	1.2	12.7/(0.1)
13-33	1	48.5	46.5	4.1	9.7	1	1.1	13.5/(0.3)
33-53	0.8	40.7	52.8	5.7	10.0	0.7	0.9	13.6/(0.4)
53-82	0.5	31.4	62.8	4.6	10.3	0.5	0.8	13.8/(0.9)
82-99	0.5	33.2	60.9	5.2	10.2	0.5	0.5	13.5/(0.6)
99-150	0.6	34.1	60	4.7	5.2	0.5	0.4	18.9/(0.3)
Pedon 7 : Gategaon (Latur) - Very fine, smectitic, isohyperthermic, Typic Haplusterts								
0-14	4.4	79.8	18	0.7	23.7	4.3	4.7	1.9/(0.6)
14-34	4.5	80.1	17.7	0.7	23.4	4.4	4.1	3.6/(0.4)
34-55	4.2	78.3	18.5	1.8	25.0	3.8	5.4	4.6/(0.4)
55-84	3.7	70.7	20.8	1.4	27.0	3.5	5.5	4.6/(0.4)
84-120	2.9	72.9	24.8	1	26.0	2.8	4.7	4.4/(0.9)
120-150+	3.1	74.3	24.4	0.6	22.3	3	5.5	7.9/(0.4)

Table 2. *Contined ...*

Depth (cm)	Exch. Ca/Mg	ECP[1]	EMP[2]	ESP[3]	WDC	Exch. Ca/(Mg+Na)	sHC cm/ hr[5]	% $CaCO_3$/ (HCO_3/Ca)
Pedon 8 : Deoni (Latur)- Very fine, smectitic, isohyperthermic, Typic Haplusterts								
0-14	1.8	62.9	34.8	0.5	22.5.	1.8	0.6	0.9/(0.7)
14-30	1.9	63.9	33.5	0.7	20.7	1.9	0.2	2.2/(0.7)
30-54	1.9	63.9	34.1	0.7	15.0	1.8	0.4	0.9/(1.0)
54-90	2	65.9	32.6	0.5	20.7	2	0.4	1.6/(1.0)
Pedon 9 : Kajal Hipperga (Latur) - Very fine, smectitic, isohyperthermic, Typic Haplusterts								
0-10	4.9	80.8	16.3	0.5	20.7	4.8	0.6	4.7/0.9
Oct-34	4.1	78.5	19.3	0.3	22.4	4	0.9	4.1/(1.5)
34-66	3.7	77.3	20.6	0.5	22.6	3.7	0.7	5.6/(1.5)
66-89	2.7	71.4	26	0.5	20.4	2.7	0.7	5.8/(0.9)
89-112	3.8	77.2	20.4	0.5	16.0	3.7	0.9	6.9/(1.8)
112-131	5.1	79.5	15.7	3.2	12.6	4.2	—	—
Pedon 10 : Bhalgaon (Aurangabad) - Fine, smectitic, isohyperthermic, Sodic Haplusterts								
0-12	1.4	47.7	34.7	12.9	18.7	1	0.2	12.3/(0.9)
Dec-33	0.9	38.5	42.9	14.8	20.4	0.7	0.01	13.5/(0.8)
33-62	0.8	32.9	40.9	22.6	28.4	0.5	0.08	14.2/(0.9)
62-88	0.8	31.3	39.2	25.4	35.4	0.5	008	14.7/(0.7)
88-123	0.6	24.4	43.7	29.1	40.4	0.3	0.01	—
123-150	0.5	19.7	40.3	37.3	38.4	0.3	0.01	12.8/(2.9)
Pedon 11 : Babhulgaon (Aurangabad) - Fine, smectitic, isohyperthermic, Sodic Haplusterts								
0-15	1.1	47.8	44.6	2.4	4.2	1	0.5	17.3/(1.5)
15-34	0.8	41	49.2	4	6.3	0.8	0.5	18.5/(1.1)
34-72	0.5	27.5	57.9	11.1	10.3	0.4	0.1	17.0/(2.3)
72-97	0.4	21.5	60.1	15.8	12.1	0.3	0.1	17.2/(1.5)
97-130	0.3	22.3	65.4	9.7	17.7	0.3	0.1	20.1/(2.3)
130-160	0.4	22.1	63	12.5	19.8	0.3	0.1	20.2/(2.3)
Pedon 12 : Patrud (Beed) - Fine, smectitic, isohyperthermic, Typic Haplusterts								
0-13	4.6	78.8	17.2	1.1	15.1	4.3	0.7	12.7/(0.4)
13-36	3.2	74.6	23.1	0.7	13.9	3.1	1.4	13.9/(0.4)
36-61	2.9	72.3	25.3	0.3	15.0	2.8	4.4	13.3/(0.1)
61-104	2.1	65.3	31.2	0.9	17.0	2	2.7	12.6/(0.2)
104-140	1.5	59.7	38.7	0.2	17.4	1.5	4.2	13.9/(0.1)
140-160	1.8	61.1	34.9	0.9	16.7.	1.7	3.4	11.8/(1.1)
Pedon 13 : Raurgaon (Beed) - Very fine, smectitic, isohyperthermic, Typic Haplusterts								
0-14	3.1	73.3	23.8	0.5	20.9	3	3.1	11.8/(1.1)
14-28	2.1	65.7	31.8	0.9	24.7	2	2.9	12.2/(1.5)
28-43	1.8	61.9	35.1	1.5	27.4	1.7	1.9	10.2/(1.5)
43-85	1.1	50.5	46.3	1.8	29.2	1.1	1.0	9.9/(2.3)
85-130	0.6	37.9	59.1	1.4	29.0	0.6	0.8	11.8/(2.1)
130-150	0.5	32.6	63	2.8	26.0	0.5	0.6	1.02/(2.0)

[1] ECP = Exchangeable calcium percentage, [2]EMP = Exchangeable magnesium percentage, [3]ESP = Exchangeable sodium percentage, [4] WDC = Water dispersible clay, [5]sHC = Saturated hydraulic conductivity

Discussions

Majority of Vertisols under study indicates that the soils have considerable amount of WDC which increases with depth (Table 2). Following the increase in clays with depth, other properties like WDC, EMP, ESP and $CaCO_3$ (Table 2) also show an increase with depth whereas exch. Ca/

Mg shows a decrease. The depth distribution of these properties point out a fact that dispersion and subsequent movement of clays have been possible in alkaline chemical environment caused by the precipitation of $CaCO_3$ at pH ≥ 8.4 (Pal *et al.*, 2003b) in semi-arid climatic conditions (Balpande *et al.*, 1996; Vaidya and Pal, 2002). Vertisols under study are mildly to strongly alkaline and are calcareous as they belong to Typic/ Sodic Haplusterts (Table 1). The absence or lesser amount of carbonate and dominance of bicarbonate in the saturation extract (Table 2) suggests that during the high evaporative demands for soil water, maintenance of a proper Ca/Mg ratio in the soil solution becomes difficult because Ca^{2+} ions get precipitated as $CaCO_3$ (Table 2). This chemical reaction causes a relative increase in EMP and ESP of soils (Table 2). This is evident from a significant positive correlation between ESP and EMP (r = 0.391 at 1% level) and also through a significant negative correlation between sHC and EMP (r = -0.483 at 1% level, Table 3). This indicates that high amount of magnesium in soils can also cause poor physical properties. Mg^{2+} ions behave more like a Na^{+} ion in impairing hydraulic properties of cracking clay soils (Balpande *et al.*, 1996). This is the opposite effect from that of saturation with Ca^{2+} ions, which leads to blocking of small pores in the soil. In other words Mg^{2+} ions are less efficient than Ca^{2+} ions in flocculating soil colloids (Rengasamy *et al.*, 1986), although the United States Salinity Research Laboratory (Richards, 1954) grouped Ca^{2+} and Mg^{2+} together with an assumption that both the ions improve soil structure. Srivastava *et al.* (2002) indicates that the formation of pedogenic $CaCO_3$ (PC) is the prime chemical reaction responsible for increasing pH, the decrease in Ca/Mg and Ca/(Mg+Na) ratios (Table 2) of exchange site with depth and in the development of subsoil sodicity.

The EMP ranged from 14 to 65 percent. In general, $CaCO_3$ content in Typic and Sodic Haplusterts (without palygorskite) increases with depth and its increase is sharper in Sodic Haplusterts than in Typic Haplusterts (Table 2). Thus the increase of EMP in general with depth is more of an effect of depletion Ca ions as $CaCO_3$ (Pal *et al.*, 2000) than by illuviation of Mg-fine clay. It is however reported that

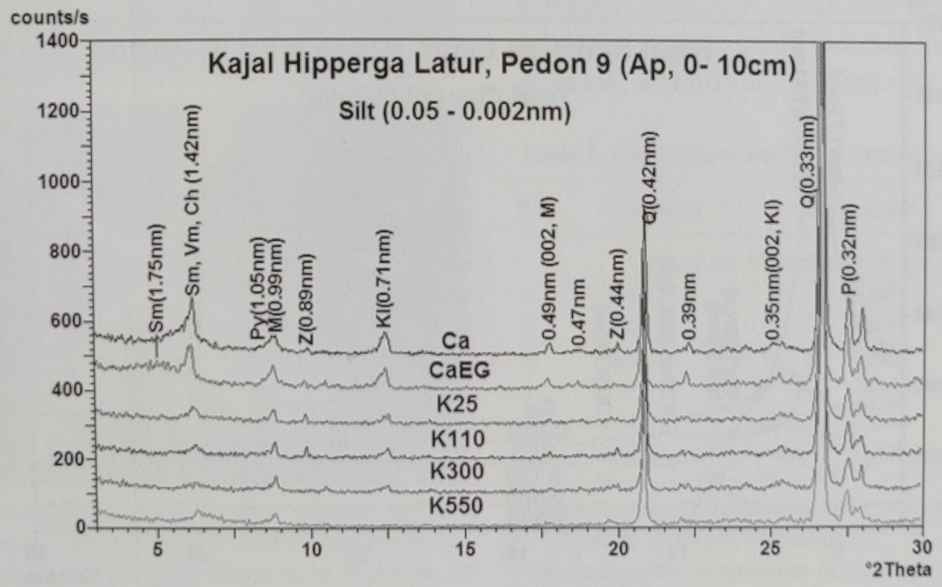

Fig. 2. *Representative XRD patterns of the silt fraction of Kajal Hipperga, Latur. Ca=Ca saturated, CaEG=Ca saturated plus glycol vapour, K25/110/300/550°C=K saturated and heated to 25°C, 110°C, 300°C and 550°C, 6NHCl= HCl treated silt, Sm=Smectite, Vm=Vermiculite, Ch=Chlorite, Py=Palygorskite, M=Mica, Kl=Kaolin, Q=Quartz,*

palygorskite particles are observed to move preferentially over smectite in the soil profile, and eventually clogs soil pores (Neaman and Singer, 2004). In palygorskite containing Typic Haplusterts (Pedons 8 and 9, Table 2), depth distribution of both exchangeable Ca/Mg showed however, a moderate decrease because of the enrichment of Ca ions provided by the Ca-zeolites, but a considerable increase in EMP with depth was observed (Table 2). However, in other Vertisols containing palygorskite (Pedons 3,6, and 10) showed a sharp decrease in Ca/Mg ratio and also a sharp increase in EMP. The depth distribution of Ca/Mg suggests that the precipitation of $CaCO_3$ as PC enhances the relative abundance of Na^+ and Mg^{2+} ions in soil exchange sites and in turn causes dispersion of fine clay smectites and the dispersed clay smectite translocated. The gradual increase in WDC with depth (Table 2) and a significant positive correlation between WDC and ESP (r = 0.397 at 1% level) support this fact. This process results in increase in EMP, ESP and $CaCO_3$ with depth (Table 2) and adversely affects the hydraulic properties of these soils. The impairment of hydraulic properties of soils is evident from significant correlations between sHC and ESP (r = -0.474), sHC and EMP (r=-0.483), $CaCO_3$ and ESP (r = 0.344), $CaCO_3$ and EMP (r= 0.598).

It is worth mentioning that, hydraulic properties of pedons 8 and 9 (Typic Haplusterts) are impaired (sHC < 10 $mmhr^{-1}$) even with very low amount of sodium on the exchange complex (ESP<<5; Table 2) and also in the presence zeolites. Mineralogical studies indicate the presence of silt and clay size palygorskite mineral with smectite, kaolinite, zeolite in pedons 8 and 9 (Figs. 2 and 3). However, the characteristic peak of palygorskite at 1.05 nm is weak, short and broad possibly because of its low content. A recent report on the presence of palygorskite in red Vertisols (Typic Haplusterts) by Kolhe *et al.* (2011) indicated its parental legacy to the red boles, sandwiched between two Deccan basalt flows. Such red Vertisols formed very close to red boles site (< than 500m) and gray Vertisols in basaltic alluvium (Pal *et al.*, 2003a), contain silt and clay size moderately sharp and broad

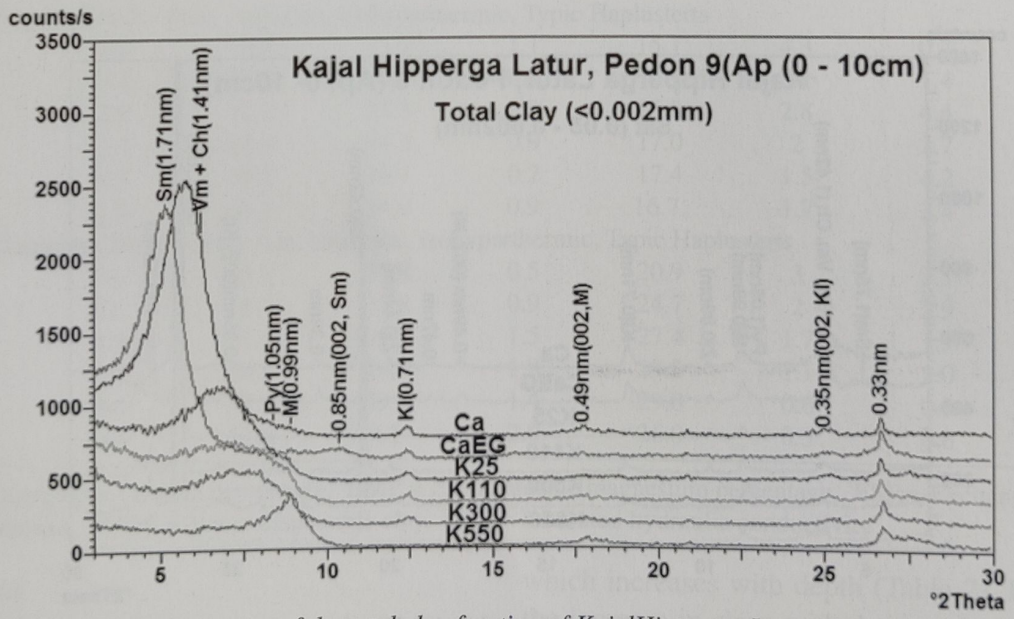

Fig. 3. Representative XRD patterns of the total clay fraction of KajalHipperga, Latur. Ca=Ca saturated, CaEG=Ca saturated plus glycol vapour, K25/110/300/550°C=K saturated and heated to 25°C, 110°C, 300°C and 550°C, Sm=Smectite, Vm=Vermiculite, Ch=Chlorite, Py=Palygorskite, M=Mica, Kl=Kaolin.

palygorskite at 1.05 nm. Palygorskite is the most magnesium-rich among the common clay minerals (Weaver and Pollard, 1973; Singer, 2002). Neaman *et al.* (1999) examined the influence of clay mineralogy on disaggregation in some palygorskite, smectite, kaolinite containing soils of the Jordan and Betshe'an Valleys in Israel. Palygorskite was observed to be the most strongly disaggregated mineral among the phyllosilicates that appear in the soil clay fraction. However, pedons 8 and 9 have ESP << 5 and Ca/Mg ratio ≥2, indicating the dominance of Ca^{2+} ion on the exchange complex. Although the naturally occurring zeolites in these soils favoured an increase in exchangeable Ca/Mg ratio, the sHC is still <1 cm hr^{-1} probably because of the much better rate of release of Mg ions from palygorskite than that of Ca ions from Ca- zeolites during the movement of water in soils. Ca-zeolites release << 1 $meqL^{-1}$ in distilled water (Pal *et al.,* 2006). Palygorskite has the strongest disaggregation potential and the highest ability to migrate in the soil among common phyllosilicates such as smectite and kaolinite. Neaman *et al.* (1999) indicated that palygorskite fibres did not associate into aggregates in soils and suspensions, even when saturated with Ca^{2+} ions. Palygorskite particles are thus likely to move preferentially over smectite and kaolinite downward in the soil profile and eventually clog soil pores (Neaman and Singer, 2004). Due to release of Mg^{+2} ions from palygorskite, the EMP often showed a higher value than ECP in Vertisols especially with ESP > 5 (Kolhe *et al.* 2011). The results of present study indicate that the adverse physical condition of Vertisols in terms of

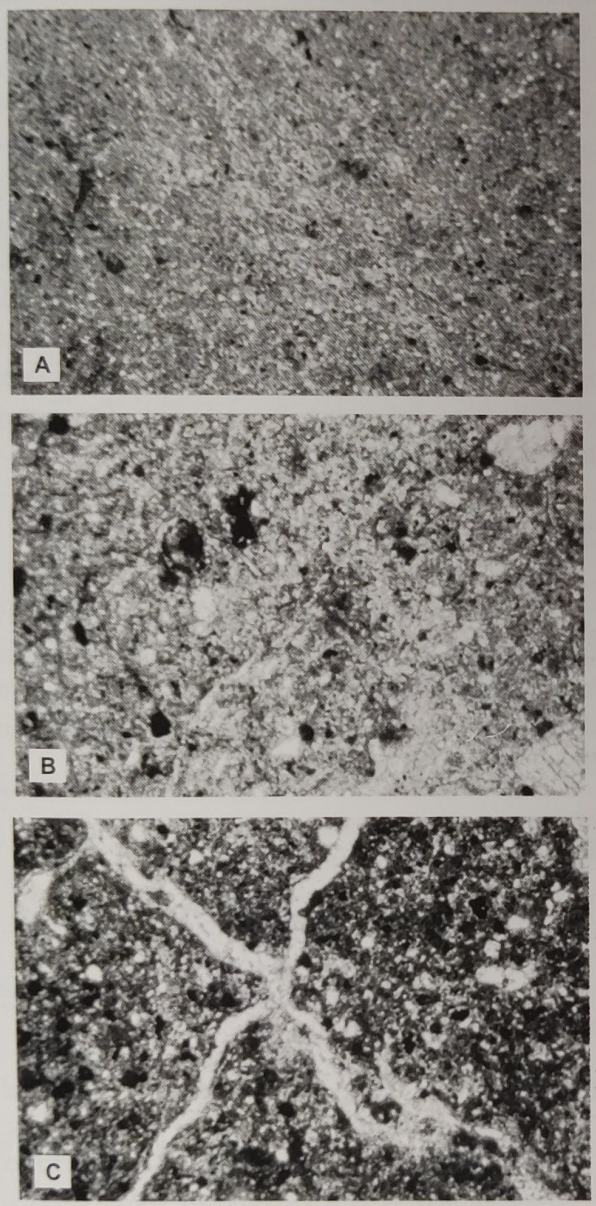

Fig. 4. *Representative photograph of plasmic fabric in cross polarized light: (a) partly unistrial and partly mosaic speckled b-fabric (Typic Haplusterts-Pedon 8, 28-36cm), (b) stipple-speckled b-fabric (Sodic Haplusterts-Pedon 3, 110-118cm),(c)crystallitic b-fabric (Sodic Haplusterts -Pedon 5, 66 –74cm).*

Table 3. Correlation coefficient between soils attributes

No.	Parameter Y	Parameter X	"r" value
	Based on 13 Pedons (75 samples)		
1	WDC[4]	ESP	r = 0.397*
2	ESP	EMP	r = 0.391 *
3	sHC[1]	EMP[2]	r = - 0.483*
4	sHC	ESP[3]	r = -0.474*
5	$CaCO_3$[5]	ESP	r = 0.344*
6	$CaCO_3$	EMP	r = 0.598*

*Correlation is significant at the 1% level.

1. Saturated hydraulic conductivity
2. Exchangeable magnesium percentage
3. Exchangeable sodium percentage
4. Water dispersible clay
5. Calcium carbonate

impairment of sHC (< 10 mm hr^{-1}) is not only due to formation of PC and concomitant development of sodicity but also due to the presence of Mg-bearing palygorskite. SAT Vertisols under study indicated that there was absence of strong plasma separation and orientation in the zone of slickenside development. The plasmic fabric of these SAT Vertisols was predominantly of granostriated, unistrial, reticulated and crystallitic in nature (Fig. 4), which indicate a weak shrink-swell of smectites that could not create the strong plasma separation with parallel striated plasmic fabrics, due to less amount of soil water that are generally made available through easy entry of rains. Despite a high degree of clay activity and shrink–swell process as manifested by high co-efficient of linear extensibility (COLE >> 0.10, Zade, 2007), soils showed weak plasma separation due to less amount of soil water for shrink-swell activity because of reduced sHC, caused by the enrichment of both ESP and EMP in Sodic Haplusterts, and EMP in Typic Haplusterts. Similar observations for Sodic Haplusterts were also made by other researchers (Kalbande *et al.*, 1992; Pal *et al.*, 2001, 2006, 2009, 2012; Vaidya and Pal, 2002). It is interesting to note that the weak plasma separation is also caused by the presence of palygorskite even though the soils are classified as Typic Haplusterts. This interaction causes drainage problems when such soils are irrigated, presenting a predicament for crop production. In view of their poor drainage conditions and loss of productivity, non-sodic Vertisols (Typic Haplusterts) with palygorskite must be considered naturally degraded soils. Similar soils may be found elsewhere in the world; thus, a new initiative to classify them is warranted (Pal *et al.*, 2012).

Conclusion

The results of the present study indicate the contemporary pedogenic processes in SAT Vertisols like the concurrent formation of pedogenic calcium carbonate and the concomitant development of sodicity are primarily responsible for the enrichment of exchangeable magnesium in the subsoils. Exchangeable Mg also causes sufficient dispersion of clay particles and blocking the macro- and micro-pores, resulting in reduced hydraulic properties in clayey and smectitic shrink-swell soils. The hydraulic properties are further impaired with the rise of exchangeable sodium level. Similar dismal hydraulic properties are also caused when SAT Vertisols contain palygorskite mineral in their silt and clay fractions. While the remedial measures to make sodic soils caused by the formation of PC and ESP are available, palygorskite containing ill-drained SAT Vertisols with high EMP need immediate research attention for their proper classification following the US Soil Taxonomy to make them resilient.

Acknowledgements

We thank Director, ICAR-NBSS and LUP, Nagpur, India for providing facilities for this work. Help received from other colleagues in the Division of Soil Resource Studies are also thankfully acknowledged.

References

Alperovitch, N., Shainberg, I. and Keren, R. 1981. Specific effect of magnesium on the hydraulic conductivity of sodic soils. *J Soil Sci.* **32**: 543-554.

Balpande, S.S. 1993. *Characteristics, genesis and degradation of Vertisols of the Purna Valley, Maharashtra*. Ph.D. thesis, Punjabrao Deshmukh Krishi Vidyapeeth, Akola (M.S.), India.

Balpande, S.S., Deshpande, S.B. and Pal, D.K. 1996. Factors and processes of soil degradation in Vertisols of Purna Valley, Maharashtra, India. *Land Deg Dev.* **7** : 313-324.

Bhattacharyya, T., Pal, D.K., Mandal, C., Chandran, P., Ray, S.K., Dipak Sarkar, Velmourougane, K., Srivastava, A., Sidhu, G.S., Singh, R.S., Sahoo, A.K., Dutta, D., Nair, K.M., Srivastava, R., Tiwary, P., Nagar, A.P. and Nimkhedkar, S.S. 2013. Soils of India: historical perspective, classification and recent advances. *Current Science.* **104** : 1308-1323.

Bullock, P., Fedoroff, N., Jongerius, A., Stoops, G. and Tursina, T. 1985.*Handbook for Soil Thin section Description*. Waine Research Walverhampton, 150.

Hillier, S. and Pharande, A. L. 2008. Contemporary pedogenic ormation of palygorskite in irrigation induced, saline-sodic, shrink-swell soils of Maharashtra, India. *Clays Clay Minr* **56**: 531–548.

Jongerius, A. and Heintzberger, G. 1975. Methods in Soil Micromorphology, A Technique for the Preparation of Large Thin Sections *Soil Survey Paper* No. 10, Netherlands Soil Survey Institute, Wageningen

Jackson, M.L. 1979. *Soil Chemical Analysis – Advanced Course,* 2nd. edn. Published by Author, University of Wisconsin MD.WI.

Kadu, P.R., Pal, D.K. and Deshpande, S.B. 1993. Effect of low exchangeable sodium on hydraulic conductivity and drainage in shrink-swell soils of Purna valley, Maharashtra. *Clay Research.* **12** : 65-70.

Kalbande, A.R., Pal, D.K. and Deshpande, S.B. 1992. *b*-fabric of some benchmark Vertisols of India in relation to their mineralogy. *J. Soil Sci.* **43** : 375-385.

Kolhe, A.H., Chandran, P., Ray, S.K., Bhattacharyya, T., Pal, D.K. and Sarkar, D. 2011. Genesis of associated Red and Black shrink-swell soils of Maharashtra. *Clay Research.* 30 : 1-11.

Neaman, A., Singer, A. and Stahr, K. 1999. Clay mineralogy as affecting disaggregation in some palygorskite-containing soils of the Jordan and Bet-She'an Valleys. *Aus. J. Soil Res.* 37 : 913-928.

Neaman, A. and Singer, A. 2004. The effects of palygorskite on chemical and physico-chemical properties of soils : a review. *Geoderma* 123 : 293-303.

Pal, D.K. and Deshpande, S.B. 1987. Characteristics and genesis of minerals in some benchmark Vertisols of India. *Pedologie.* 37**:** 259-275.

Pal, D.K., Dasog, G.S., Vadivelu, S., Ahuja, R.L., Bhattacharyya, T. 2000. Secondary calcium carbonate in soils of arid andsemi-arid regions of India. In: Lal, R., Kimble, J.M., Eswaran,H., Stewart, B.A. (Eds.), Global Climate Change and Pedogenic Carbonates. Lewis Publishers, Boca Raton, FL,pp. 149–185.

Pal, D.K., Balpande, S.S. and Srivastava, P. 2001. Polygenetic Vertisolsof the Purna Valley of central India. *Catena.* **43**: 231–249.

Pal, D.K., Bhattacharyya, T., Ray, S.K., Bhuse, S.R. 2003a. Developing a model on the formation and resilience of naturally degraded black soils of the Peninsular India as a decision support system for better land use planning. *NRDMS, DST Project Report,* NBSSLUP (ICAR), Nagpur, 144p.

Pal, D.K., Srivastava, P. and Bhattacharyya, T. 2003b. Clay illuviation in calcareous soils of the semi-arid part of the Indo-Gangetic plains, India. *Geoderma.* **115** : 177-192.

Pal, D.K., Bhattacharyya, T., Ray, S.K., Chandran, P., Srivastava, P., Durge, S.L. and Bhuse, S.R. 2006. Significance of soil modifiers (Ca-zeolites and gypsum) in naturally degraded Vertisols of the peninsular India in redefining the sodic soils. *Geoderma.* **136** : 210–228.

Pal, D.K., Bhattacharyya, T., Chandran, P., Ray S.K., Satyavathi, P.L.A., Durge, S.L., Raja,

P. and Maurya, U.K. 2009. Vertisols (cracking clay soils) in a climosequence of Peninsular India: evidence for Holocene climate changes. *Quaternary International* **209**: 6-21

Pal, D.K., Wani, S.P. and Sahrawat, K.L. 2012. Vertisols of tropical Indian environments: Pedology and edaphology. *Geoderma* 189-190: 28-49

Piper, C.S. 1950. *Soil and Plant Analysis*. The University of Adelaide, Adelaide, 368p.

Richards, E.A. 1954. *Diagnosis and improvement of saline and alkali soils.* Agriculture Hand Book No. 60, United States Salinity Laboratory, United States Dept. of Agriculture.

Rengasamy, P., Greene R.S.B. Ford G.W. 1986. Influence of magnesium on aggregate stability in sodic red-brown earths. *Aus. J. Soil Res.* **24**: 229-237.

Singer, A. 2002. *Palygorskite and sepiolite. In : Dixon, J.B. Schulze, D.G. (Eds.), Soil Mineralogy with Environmental Applications.* SSSA Book Series, Vol. 7. Soil Science Society of America, Madison, WI, pp.555-583.

Sombroek, W.G. 1981. The use of palygorskite as diagnostic criteria in soil classification. *Pedologie* **31**, 121.

Soil Survey Division Staff.1993. *Soil Survey Manual.* USDA Agriculture, Handbook No.18, (Department of Agriculture: Washington, DC).

Soil Survey Staff, 1999. *Soil Taxonomy : a basic system of soil classification for making and interpreting soil surveys.* Agri. Handbook, USDA, 436, p. 869.

Soil Survey Staff, 2014. *Keys to Soil Taxonomy* (12theds) United States Department of Agriculture Natural Resources Conservation Service, 362p

Srivastava, P., Bhattacharyya, T. and Pal, D.K. 2002. Significance of the formation of calcium carbonates minerals in the pedogenesis and management of cracking clay soils (Vertisols) of India. *Clays Clay Miner* **50**: 111-126.

Vaidya, P.H. and Pal, D.K. 2002. Microtopography as a factor in the degradation of Vertisols in central India. *Land Deg Devt.* **13** : 429-445.

Weavers, C.E. and Polland, L.E. 1973. *The chemistry of clay minerals. Developments in Sedimentology,* Vol. 15, Elsevier, Amsterdam, Netherlands.

Zade, S. P. 2007. *Pedogenetic Studies of Some Deep Shrink-Swell Soils of Marathwada Region Of Maharashtra to Develop a Viable Land Use Plan.* Ph.D. Thesis. Dr. P.D.K.V. Akola, Maharashtra, India.

(Received 28th June , 2017; Accepted October 2017)

ACKNOWLEDGEMENT

I grate fully acknowledge the help received from the followings scientists /Professors who reviewed the manuscripts for 2016 issue.

1. Dr Padikkal Chandran
2. Dr Sanjay Ray
3. Dr Goutam Goswami
4. Dr Siddhartha Mukhopadhyay
5. Dr K.M Manjaiah

INSTRUCTIONS FOR CONTRIBUTORS

CLAY RESEARCH is the official publication ofTHE CLAY MINERALS SOCIETY OF INDIA and is published twice a year, in June and December. The Journal undertakes to publish articles of interest to the international community of clay scientists, and will cover the subject areas of mineralogy, geology and geochemistry, crystallography, physical and colloid chemistry, physics, ceramics, civil and petroleum engineering and soil science.

The Journal is reviewed in *Chemical Abstracts, MineralogicalAbstracts, and Soils and Fertilizers.*

Paper (in English) should be submitted to the Editor, Clay Research **"The Clay Minerals Society of India"** Division of Soil Science and Agricultural Chemistry, I.A.R.I., New Delhi-I to 012. E-mail: samar_I953@yahoo.com. At least one of the authors should be member of THE CLAY MINERALS SOCIETY OF INDIA. Submission is an undertaking that the manuscript has not been published or submitted for publication elsewhere.

Manuscripts should not exceed sixteen typed (double spaced) pages including tables and illustrations. **The original and two copies oftext and illustrations should be submitted.**

Form Manusciprts should be typewritten, double spaced on white paper, with wide margins. Intending contributors should consult a recent issue of CLAY RESEARCH for the standard format and style. The manuscript should have the sections ABSTRACT, introductory portion (untitled), MATERIALS AND METHODS, RESULTS and DISCUSSION and REFERENCES.

Title page should contain manuscript title, full name(s) of author(s), address (es) of the institution(s) of the author(s), a short running title not exceeding 60 characters including spaces, footnotes if any to the title, and complete mailing address of the person to whom communications should be sent.

Abstract should be a condensation of the ideas and results of the paper. It should not exceed 25'0 words. Do not make reference to the literature in the abstract.

Tables should have the simplest possible column headings. Type each table on a separate page; indicate location in the text by marking in the margin of text page.

Figures should be self-illustrative, drawn with black India ink on tracing paper or white Board. The lattering should be large enough to permit size reduction to one Journal page column width (about 7.0 cm) without sacrificing legibility. **The original tracing should be submitted**. The size of the drawing should not exceed 24 × 17 cm. Give the numbered legend on a separate sheet, not on the figure itself. Data available in the tables should not be duplicated in the form of illustrations. Indicate the location of the figure in the text by marking in the margin of the page.

Photographs should be in the form of glossy prints with strong contrast. In photomicrographs, the scale in micron or other suitable unit should be drawn on the print. Give the numbered legend on a separate sheet. Indicate the location of the photograph in the text by making in the margin of the text page.

References should be cited in the text by the name(s) of author(s) if two or less, and year of publication. If there are more than two authors, give the name ofthe first author followed by *'et al'* and year. Full references giving author(s) and initial(s), year, title of paper, (journal, volume, number if paged separately), first and last pages should be listed alphabetically at the end of the paper. Journal title should be abbreviated in accordance with the World List of Scientific Periodicals and its sequences. Examples are

Grim, R.E., Bray, R.H. and Bradley, W.R. 1937. The mica in argillaceous sediments. *Am. Miner.* **22**:813-829.

Brindley, G.W. 1961. Chlorite minerals. In *(G.* Brown, Ed.) *The X-ray Identification and Crystal Structures of Clay Minerals,* Mineralogical Society, London, pp.242-296.

Theng, B.K.G. 1974. *The Chemistry of Clay Organic Reactions,* Adam. Hilger, London, 343 pp.

Review Every manuscript submitted to CLAY RESEARCH is independently reviewed by one or more referees. Acceptance or rejection of a manuscript is the responsibility of the Editor.

Reprints No free reprints are supplied to authors. Order for priced reprints should be sent when required by the Editor.

Clay Research

Vol. 36 **June 2017** **No. 1**

CONTENTS

Printed at : Cambridge Printing Works, New Delhi-1100028. (Mobile : 9811860113)